PERFORMANCE OF A UTC FW-4S SOLID-PROPELLANT ROCKET MOTOR UNDER THE COMBINED EFFECTS OF SIMULATED ALTITUDE AND ROTATIONAL SPIN

H. L. Merryman and L. R. Smith
ARO, Inc.

ENGINE TEST FACILITY
ARNOLD ENGINEERING DEVELOPMENT CENTER
AIR FORCE SYSTEMS COMMAND
. ARNOLD AIR FORCE STATION, TENNESSEE 37389

December 1974

Final Report for Test Conducted on April 11, 1974

Approved for public release; distribution unlimited.

NOTICES

When U. S. Government drawings specifications, or other data are used for any purpose other than a definitely related Government procurement operation, the Government thereby incurs no responsibility nor any obligation whatsoever, and the fact that the Government may have formulated, furnished, or in any way supplied the said drawings, specifications, or other data, is not to be regarded by implication or otherwise, or in any manner licensing the holder or any other person or corporation, or conveying any rights or permission to manufacture, use, or sell any patented invention that may in any way be related thereto.

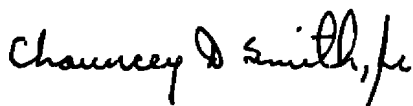Qualified users may obtain copies of this report from the Defense Documentation Center.

References to named commercial products in this report are not to be considered in any sense as an endorsement of the product by the United States Air Force or the Government.

This report has been reviewed by the Information Office (OI) and is releasable to the National Technical Information Service (NTIS). At NTIS, it will be available to the general public, including foreign nations.

APPROVAL STATEMENT

This technical report has been reviewed and is approved for publication.

FOR THE COMMANDER

CHAUNCEY D. SMITH, JR.
Lt Colonel, USAF
Chief Air Force Test Director, ETF
Directorate of Test

FRANK J. PASSARELLO
Colonel, USAF
Director of Test

UNCLASSIFIED

REPORT DOCUMENTATION PAGE		READ INSTRUCTIONS BEFORE COMPLETING FORM
1. REPORT NUMBER AEDC-TR-74-83	2. GOVT ACCESSION NO.	3. RECIPIENT'S CATALOG NUMBER
4. TITLE (and Subtitle) PERFORMANCE OF A UTC FW-4S SOLID- PROPELLANT ROCKET MOTOR UNDER THE COMBINED EFFECTS OF SIMULATED ALTITUDE AND ROTATIONAL SPIN		5. TYPE OF REPORT & PERIOD COVERED Final Report - April 11, 1974
		6. PERFORMING ORG. REPORT NUMBER
7. AUTHOR(s) H. L. Merryman and L. R. Smith - ARO, Inc.		8. CONTRACT OR GRANT NUMBER(s)
9. PERFORMING ORGANIZATION NAME AND ADDRESS Arnold Engineering Development Center Arnold Air Force Station Tennessee 37389		10. PROGRAM ELEMENT, PROJECT, TASK AREA & WORK UNIT NUMBERS Program Element 921E5
11. CONTROLLING OFFICE NAME AND ADDRESS National Aeronautics and Space Administration (LRC), Scout Project Office, Hampton, Virginia 23365		12. REPORT DATE December 1974
		13. NUMBER OF PAGES 40
14. MONITORING AGENCY NAME & ADDRESS(if different from Controlling Office)		15. SECURITY CLASS. (of this report) UNCLASSIFIED
		15a. DECLASSIFICATION/DOWNGRADING SCHEDULE N/A
16. DISTRIBUTION STATEMENT (of this Report) Approved for public release; distribution unlimited.		
17. DISTRIBUTION STATEMENT (of the abstract entered in Block 20, if different from Report)		
18. SUPPLEMENTARY NOTES Available in DDC		
19. KEY WORDS (Continue on reverse side if necessary and identify by block number) FW-4S motors ballistics rocket motors structural integrity solid propellants specific impulse altitude tests total impulse		

20. ABSTRACT (Continue on reverse side if necessary and identify by block number)

One United Technology Center FW-4S solid-propellant rocket motor was fired at an average simulated altitude of 103,000 ft while spinning about its axial centerline at 180 rpm. The objectives of the test program were to determine motor altitude ballistic performance including the measurement of the nonaxial thrust vector and to demonstrate structural integrity of the motor case and nozzle. These objectives are presented and discussed.

DD FORM 1473 EDITION OF 1 NOV 65 IS OBSOLETE
1 JAN 73

UNCLASSIFIED

PREFACE

The work reported herein was conducted by the Arnold Engineering Development Center (AEDC), Air Force Systems Command (AFSC), at the request of the National Aeronautics and Space Administration for United Technology Center, under Program Element 921E5. The results were obtained by ARO, Inc. (a subsidiary of Sverdrup & Parcel and Associates, Inc.), contract operator of the AEDC, AFSC, Arnold Air Force Station, Tennessee. The work was conducted in Propulsion Development Test Cell (T-3) of the Engine Test Facility (ETF) under ARO Project No. RA307. Data reduction was completed on April 26, 1974, and the manuscript (ARO-ETF-TR-74-55) was submitted for publication on July 10, 1974.

CONTENTS

ILLUSTRATIONS

TABLES

1.0 INTRODUCTION

The United Technology Center (UTC) FW-4S rocket motor is used as the propulsion unit for the forth stage of NASA's Scout launch vehicle. The test program reported herein was conducted to determine the altitude performance of motor S/N 2501-2, which will be used to determine the acceptability of four flight motors. The FW-4S is similar to the Thiokol Chemical Corporation TE-M-640 motor, two of which were tested at the AEDC previously, also under ARO Project No. RA307. Both the UTC FW-4S motor and TCC TE-M-640 motor carry the NASA Scout designation Altair IIIA.

The test objectives of this program were to determine the motor altitude ballistic performance, including measurement of the nonaxial thrust vector, and to demonstrate structural integrity of the FW-4S rocket motor when fired while spinning about its axial centerline at 180 rpm.

Motor ignition characteristics, altitude ballistic performance, structural integrity of the motor case and nozzle, and nonaxial thrust vector data are presented and discussed.

2.0 APPARATUS

2.1 TEST ARTICLE

The UTC FW-4S motor (Fig. 1) is a flightweight solid-propellant rocket motor. The outside diameter of the motor is 19.67 in., and the overall length is 58.45 in. The 40.38-in.-long chamber is a filament-wound glass fiber and epoxy resin structure, nominally 0.08 in. thick, with a 27-in.-long cylindrical section and with ovaloid forward and aft domes which incorporate adapters of high-strength aluminum. The domes terminate in aluminum polar bosses for igniter and nozzle installation. The chamber is filament-wound directly over a semi-destructible mandrel, which supports the silica-loaded Buna-N® rubber insulator.

The nozzle assembly (Fig. 1a) consists of an Graph-I-Tite® G-90 throat insert with a nominal throat area of 4.30 in.² and an expansion cone comprised of silica phenolic backed with a steel shell to provide structural rigidity. Graphite cloth is bonded to the silica phenolic over an area from the graphite throat insert to an area ratio of 9:1. The nominal area ratio is 50:1, and the expansion half-angle is 20 deg. The nozzle assembly is flanged and bolted to the motor case aft polar boss flange.

The loaded motor weighs approximately 660 lbm, of which nominally 605 lbm is propellant. The composite propellant grain (UTP 3096A) is a case-bonded, transversely slotted tube configuration (Fig. 1a). Nominal motor performance is: thrust, 5730 lbf; chamber pressure, 780 psia; and action time, 30.2 sec.

Ignition was accomplished by an igniter (Fig. 2) which contained 0.16 lbm of UTP 1095 propellant. The igniter used one double-bridgewire SD60A-1, nominal 6-sec-delay squib to ignite a 5.0-gm boron-potassium nitrate ($BKNO_3$) pellet charge, which in turn initiated burning within the igniter. The $BKNO_3$ pellets are held in position by a pellet retainer screen. Two squib ports are available, only one of which was used; the igniter also contains two chamber pressure ports.

.2.2 INSTALLATION

The motor was cantilever mounted to the spindle face of a spin-fixture assembly in Propulsion Development Test Cell (T-3). The spin assembly was mounted on a thrust cradle, which was supported from the cradle support stand by three vertical and two horizontal double-flexure columns (Fig. 3). The spin-fixture assembly consists of a 10-hp squirrel-cage-type drive motor, a thrust bearing assembly, a 46-in.-long spindle having a 36-in.-diam aft spindle face, and a 170-channel slip-ring assembly.

The motor was rotated counterclockwise, looking upstream, during the firing. Electrical leads to and from the igniter, chamber pressure transducers, and thermocouples were provided through the slip-ring assembly mounted between the forward and aft bearing assemblies on the spindle. Axial thrust was transmitted through the spindle-thrust bearing assembly to two load cells mounted just forward of the thrust bearing.

Preignition pressure altitude conditions were maintained in the test cell by a steam ejector operating in series with the ETF exhaust gas compressors. During the motor firing, the motor exhaust gases were used as the driving gas for the 32-in.-diam, ejector-diffuser system to maintain test cell pressure at an acceptable level.

2.3 INSTRUMENTATION

Instrumentation was provided to measure axial thrust, motor chamber pressure, lateral force, aft dome strain, test cell pressure, motor case and nozzle temperatures, and motor rotational speed. Table 1 presents instrument ranges, recording methods, and an estimate of measurement uncertainty over the range of measurement for all reported parameters.

The axial thrust measuring system consisted of two double-bridge, strain-gage-type load cells mounted in series with the axial double-flexure column forward of the thrust bearing on the motor centerline. The lateral (nonaxial) force measuring system consisted of two double-bridge, strain-gage-type load cells installed forward and aft between the flexure-mounted cradle and the cradle support stand normal to the motor axial centerline and in the horizontal plane passing through the motor axial centerline (Fig. 3).

Bonded strain-gage-type transducers were used to measure motor chamber pressure (0 to 1000 and 0 to 15 psia). Chromel®-Alumel® (CA) thermocouples were used to measure motor chamber and nozzle temperatures during and after the motor burn time. The thermocouple locations are shown in Fig. 4. Six strain grids were bonded to the motor case on the aft dome (Fig. 5) to measure strain (deflection) during motor operation. Unbonded strain-gage-type transducers were used to measure test cell pressure. Motor rotational speed and angular orientation with time were determined from the output of a magnetic pickup.

The output signal of each measuring device was recorded on independent instrumentation channels. The instrument outputs were recorded on magnetic tapes from a multi-input, analog-to-digital converter for reduction at a later time by an electronic digital computer. The thrust chamber pressure, and test cell pressure data channels were recorded at 1248 samples per second. The thermocouples and strain grids were recorded at 25 samples per second.

The output signal from the magnetic rotational speed pickup was recorded in the following manner: A frequency-to-analog converter was triggered by the pulse output from the magnetic pickup and in turn supplied a square wave of constant amplitude to the electronic counter and magnetic tape. The scan sequence of the electronic counter was adjusted so that it displayed directly the motor spin rate in revolutions per minute.

The millivolt outputs of the lateral force load cells were recorded on magnetic tape from a multi-input, analog-to-digital converter at a sampling rate of 2500 samples per second.

Selected channels of thrust and pressures were recorded on null-balance, potentiometer-type charts for analysis immediately after a motor firing. High-speed, motion-picture cameras provided a permanent visual record of the firing.

2.4 CALIBRATION

The thrust calibration weights, thrust load cells, and pressure transducers were laboratory calibrated prior to usage in this test. After installation of the measuring devices in the test cell, the systems were again calibrated at sea-level, nonspin, ambient conditions and at simulated altitude while spinning at 180 rpm.

The pressure and lateral force recording systems were calibrated by an electrical, four-step calibration, using resistance in the transducer circuits to simulate selected pressure levels. The axial thrust instrumentation systems were calibrated by applying to the thrust cradle known forces, which were produced by deadweights acting through a bell crank.

7

The calibrator is hydraulically actuated and remotely operated from the control room. Thermocouple recording instruments were calibrated by using known millivolt levels to simulate thermocouple outputs.

After the motor firing, with the test cell still at simulated altitude pressure, the recording systems were recalibrated to determine any shift.

3.0 PROCEDURE

The UTC FW-4S rocket motor arrived at AEDC on March 18, 1974. The motor was visually inspected for possible shipping damage and radiographically inspected for grain cracks, voids, or separations and found to meet criteria provided by the manufacturer. During storage in an area temperature conditioned at 75 ± 5°F, the motor assembly was weighed, the nozzle throat and exit diameters were measured, and the motor was installed in the firing hardware. Before installation in the test cell, the motor assembly was temperature conditioned at 75 ± 5°F for a minimum of 40 hr.

After installation of the motor assembly in the test cell, the motor centerline was axially aligned with the spin axis by rotating the motor assembly and measuring the deflection of the nozzle throat flange and nozzle exit and making appropriate adjustments. Instrumentation connections were made, and the motor was balanced while spinning at 180 rpm. The initiator was installed in the igniter, and a continuity check of all electrical systems was performed. Prefire, sea-level calibrations were completed, and the test cell pressure was reduced to the desired altitude condition. Spinning of the motor was started, and after spinning had stabilized, a complete set of altitude calibrations was taken.

The final operation prior to firing was to adjust the circuit resistance and voltage to provide 10 amps to the igniter squib. The entire instrumentation measuring-recording complex was activated, and the motor was fired while spinning (under power) at 180 rpm. After motor tailoff, the spinning was maintained for 1500 sec while postfire temperature scans and altitude calibrations were accomplished. The unit was then decelerated slowly until rotation had stopped and the test cell pressure was returned to ambient conditions. The motor was inspected, photographed, and removed to the storage area. Postfire inspections consisted of measuring the nozzle, weighing the motor, and photographically recording the postfire condition of the motor.

4.0 RESULTS AND DISCUSSION

One United Technology Center (UTC) FW-4S solid-propellant rocket motor (S/N 2501-2) was fired in Propulsion Development Test Cell (T-3). The motor was tested at an average pressure altitude of 103,000 ft while spinning about its axial centerline at

180 rpm. The objectives of the program were to determine motor altitude ballistic performance, including the measurement of the nonaxial thrust vector, and to demonstrate structural integrity of the motor when tested under the combined effects of rotational spin and near-vacuum environment at $75 \pm 5°F$.

The resulting data are presented in both tabular and graphical form. Motor performance data are presented in Table 2, and motor physical dimensions are summarized in Table 3. Nonaxial thrust data are presented and discussed. Altitude ignition characteristics and ballistic performance are also presented. When multiple channels of equal accuracy instrumentation data were used to obtain values of a single parameter, the average values were used to calculate the data presented.

4.1 ALTITUDE IGNITION CHARACTERISTICS

The motor ignited at a pressure altitude of about 121,000 ft. Ignition delay time, defined as the time interval from the first indication of chamber pressure until chamber pressure has risen to 90 percent of maximum, was 0.12 sec. This was within the specified limits of 0.071 to 0.165 sec.

4.2 ALTITUDE BALLISTIC PERFORMANCE

The variations of thrust, chamber pressure, and test cell pressure with time are presented in Fig. 6. Twice during the firing a momentary increase in test cell pressure was experienced caused by exhaust gas recirculation. This occurrence was experienced at the ETF in a previous test of an FW-5 motor but had not been previously encountered during the FW-4S firing.

Since the nozzle does not operate fully expanded at the low chamber pressures encountered during tailoff, the measured total impulse data during this period cannot be corrected to vacuum conditions by adding the product of the cell pressure integral and nozzle exit area. Therefore, total burn time and action time were segmented, and the method used to determine vacuum impulse is illustrated in Fig. 7. The exhaust nozzle flow breakdown was considered to have occurred simultaneously with the exhaust diffuser flow breakdown (as indicated by a rapid increase in cell pressure during tailoff). The flow at the nozzle throat was considered sonic until the ratio of chamber-to-cell pressure had decreased to a value of 1.3 (Fig. 8).

Action time (t_a), defined as the time interval between 10 percent of maximum chamber pressure during ignition and 10 percent of maximum chamber pressure during tailoff, was 31.12 sec and within the specified limits of 28.4 to 32.0 sec. Web burnout time (t_{wb}), defined as the time abscissa at the intersection of the chamber pressure-time

curve with the bisector of the angle between the tangents of the final level portion of the chamber pressure-time curve and of the descending portion of the curve, was about 29.3 sec. There was no specified limit on web burnout time. Total burn time (t_s), defined as the time interval between the first indication of chamber pressure during ignition and the time at which the ratio of chamber-to-cell pressure had decreased to 1.3 during tailoff, was approximately 126 sec. Nozzle flow breakdown time (t_{bd}), the time after ignition when exhaust diffuser flow breakdown occurs as indicated by an abrupt increase in cell pressure during tailoff, was 30.87 sec.

Vacuum total impulse (based on t_a) was 170,935 lbf-sec and was below the specification minimum value of 171,600 lbf-sec. Vacuum total impulse (based on t_s) was 172,024 lbf sec, and vacuum specific impulse (based on t_s and the manufacturer's stated propellant weight) was 284.34 lbf-sec/lbm. Ten lbm of propellant residue (alumium oxide) remained inside the motor case after the firing. Table 4 presents a comparison of performance of this motor with the previous FW-4S motor tested at AEDC.

4.3 NONAXIAL THRUST VECTOR MEASUREMENT

Measurement of motor thrust misalignment was accomplished by measuring the nonaxial (lateral) component of the axial thrust. The recorded lateral thrust data were corrected for installation and/or electronic effects as described in Ref. 1. The resulting data are presented in Fig. 9.

The maximum magnitude of nonaxial thrust recorded during the near steady-state portion of motor operation was 25.7 lbf and occurred 10 sec after the first indication of chamber pressure. The corresponding angular position of the nonaxial thrust vector (measured clockwise, looking upstream) was 15 deg. The average magnitude of the nonaxial thrust vector during the firing was about 16 lbf.

Based on pretest dynamic calibrations, the estimated uncertainty of the nonaxial force measurements during the near steady-state portion of motor operation was about ±0.5 lbf.

4.4 STRUCTURAL INTEGRITY

Motor case and nozzle temperature variations with time are presented in Fig. 10. The Model Specification (Ref. 2) requires that the case temperature be below 500°F between web burnout $(t_{wb} = 29.3$ sec) and 200 sec after web burnout. The temperature measured by thermocouples T5 and T6 exceeded this specified maximum by about 90 and 100°F, respectively, (Fig. 10b). The maximum measured motor case temperature (T6, Fig. 4) was about 660°F and occurred about 481 sec after web burnout (Fig. 10b). The maximum measured nozzle temperature (T12 Fig. 4) was about 790°F and occurred about 101 sec after web burnout (Fig. 10e).

Variation of motor case aft dome strain with time is presented in Fig. 11. Maximum motor case strain during the near steady-state portion of motor operation (excluding the initial spike) was +1427 μ in./in. (tension) and occurred approximately 16.5 sec after the first indication of chamber pressure (SGR-2, Fig. 11b).

Postfire examination revealed discoloration and delaminations (Fig. 12) in the motor case which are attributed to the high motor case temperatures. Almost all the insulation was charred away from the case in all areas. Postfire condition of the nozzle was visually satisfactory.

Posttest information from United Technology Center indicated that approximately 10 lbm of aluminum oxide remained inside the motor case. The aluminum oxide had been uniformly distributed against the inside of the motor case during spinning. When rotation of the motor had terminated, the cooled oxide "slag" cracked and fell down to the bottom of the motor case. The prefire unbalance was only slightly affected, changing from 2.6 lb at a location of 237 deg (looking upstream) to a postfire unbalance of 1.8 lb at 249 deg.

5.0 SUMMARY OF RESULTS

One United Technology Center FW-4S solid-propellant rocket motor was tested to determine motor altitude ballistic performance, including the measurement of the nonaxial thrust vector, and to demonstrate the structural integrity of the motor case and nozzle under the combined effects of rotational spin and simulated altitude conditions while spinning about its axial centerline at 180 rpm. The results are summarized as follows:
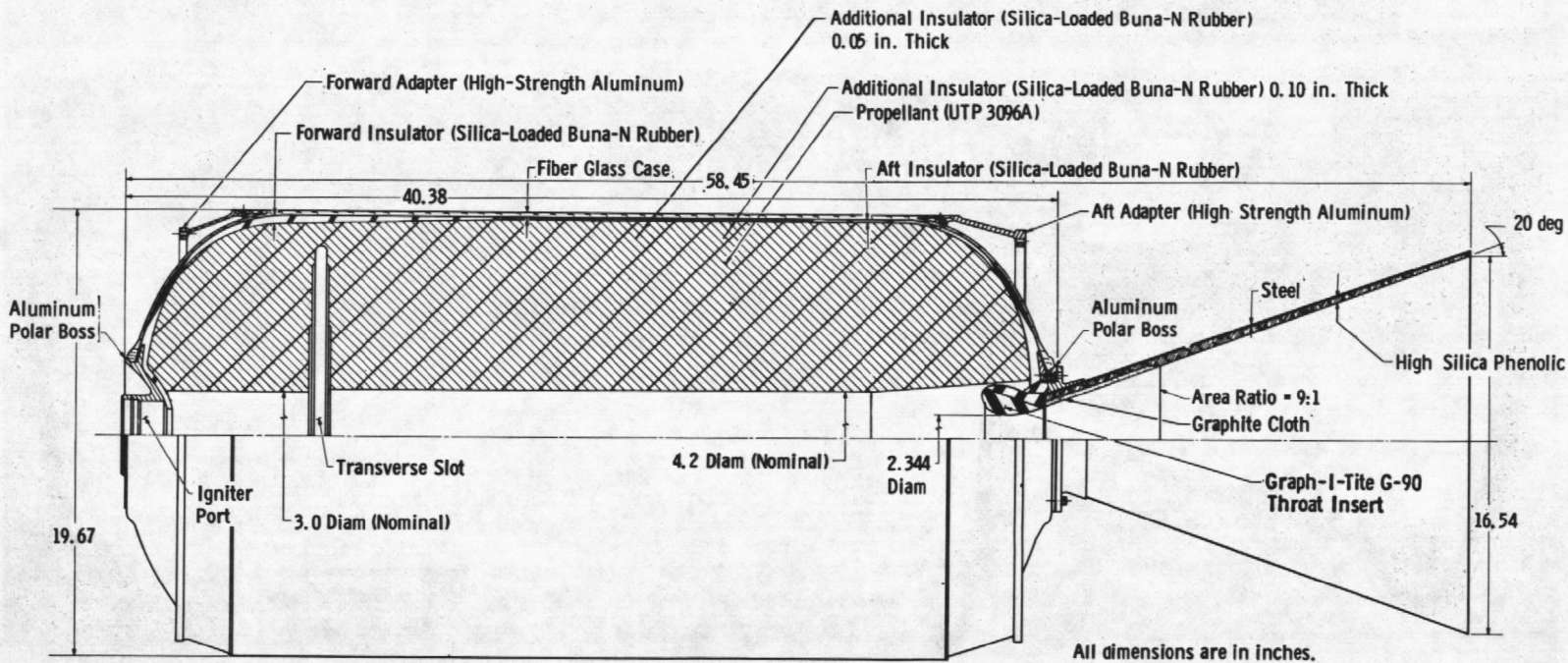
1. Ignition delay time, the time interval from first indication of chamber pressure until chamber pressure has risen to 90 percent of maximum, was 0.12 sec. This was within the specified limits of from 0.071 to 0.165 sec.

2. Action time, the time interval between 10 percent of maximum chamber pressure during ignition and 10 percent of maximum chamber pressure during tailoff, was 31.12 sec. This was within the specified limits of from 28.4 to 32.0 sec.

3. Total burn time, the time interval between the first indication of chamber pressure during ignition and the time at which the ratio of chamber-to-cell pressure had decreased to 1.3 during tailoff, was approximately 126 sec. There were no specified limits on total burn time.

4. Web burnout time, the time abscissa at the intersection of the chamber pressure-time curve with the bisector of the angle between the tangents

of the final level portion of the chamber pressure-time curve and of the descending portion of the curve, was about 29.3 sec. There were no specified limits on this time interval.

5. Vacuum total impulse based on t_a was 170,935 lbf-sec and was below the specification minimum value of 171,600 lbf-sec. Vacuum total impulse based on t_s was 172,024 lbf-sec; there were no specified limits on this parameter.

6. Vacuum specific impulse, based on total burn time and the manufacturer's stated propellant weight, was 284.34 lbf-sec/lbm.

7. The maximum magnitude of nonaxial thrust recorded during the near steady-state portion of motor operation was 25.7 lbf and occurred 10 sec after the first indication of chamber pressure. The average magnitude of the nonaxial thrust vector was about 16 lbf.

8. The motor case temperature exceeded the Model Specification maximum by as much as 100°F during the 200 sec following web burnout. The maximum measured motor case temperature was 660°F and occurred about 481 sec after web burnout. The maximum measured nozzle temperature was 790°F and occurred about 101 sec after web burnout. There were no specified limits on nozzle temperature.

9. Maximum motor strain was 1427 μ in./in. (tension) and occurred about 16.5 sec after the first indication of chamber pressure. There were no specified limits on motor strain.

10. Postfire examination revealed discoloration and delaminations in the motor case which resulted from abnormally high temperatures (in excess of 500°F). Postfire condition of the nozzle was visually satisfactory.

11. Approximately 10 lbm of residual propellant (aluminum oxide) remained in the case as a slag which had cracked upon cooling and had fallen to the bottom of the motor case following termination of the motor rotation.
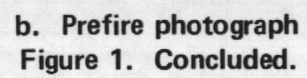
REFERENCES

1. Nelius, M. A. and Harris, J. E. "Measurements of Nonaxial Forces Produced by Solid-Propellant Rocket Motors Using a Spin Technique." AEDC-TR-65-228 (AD474410), November 1965.

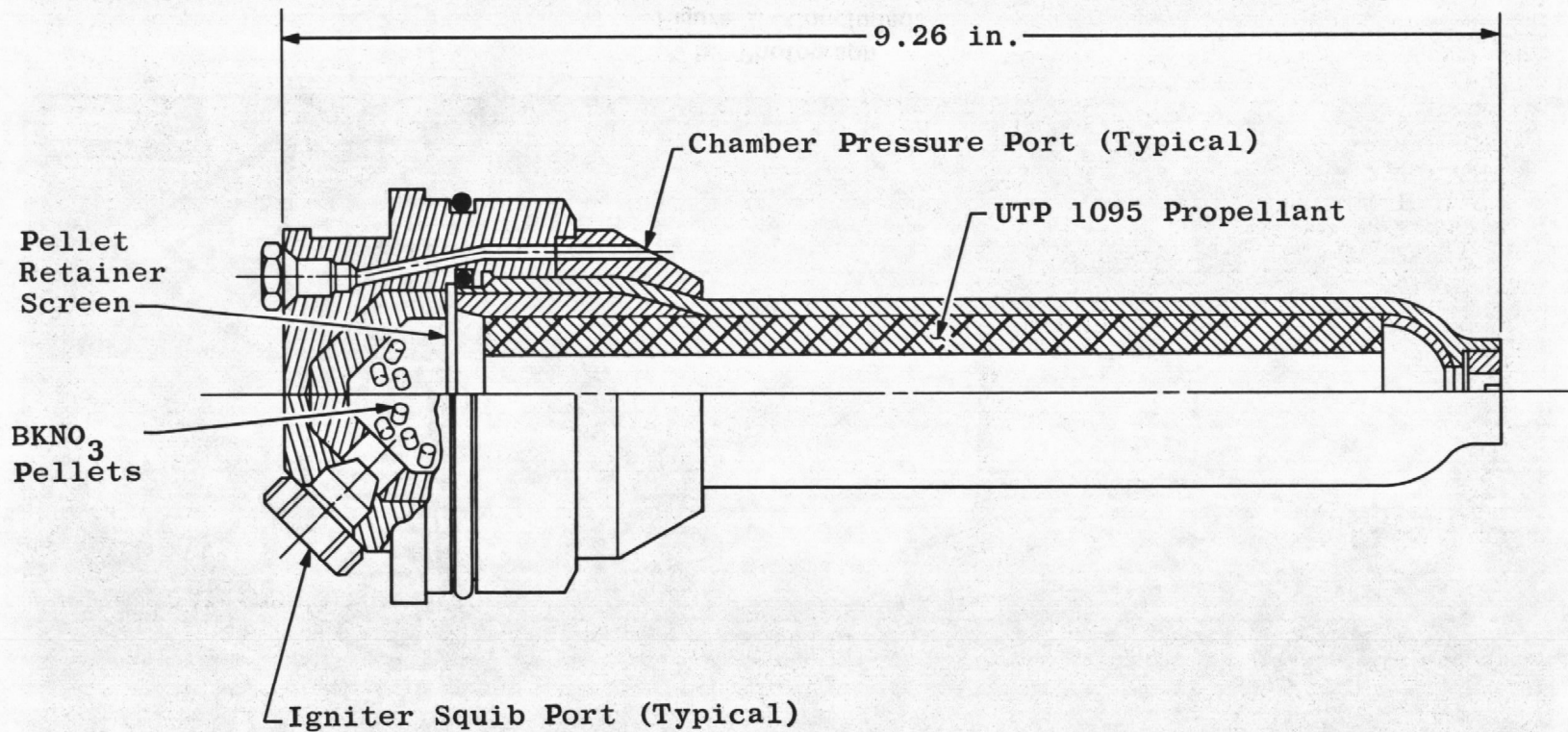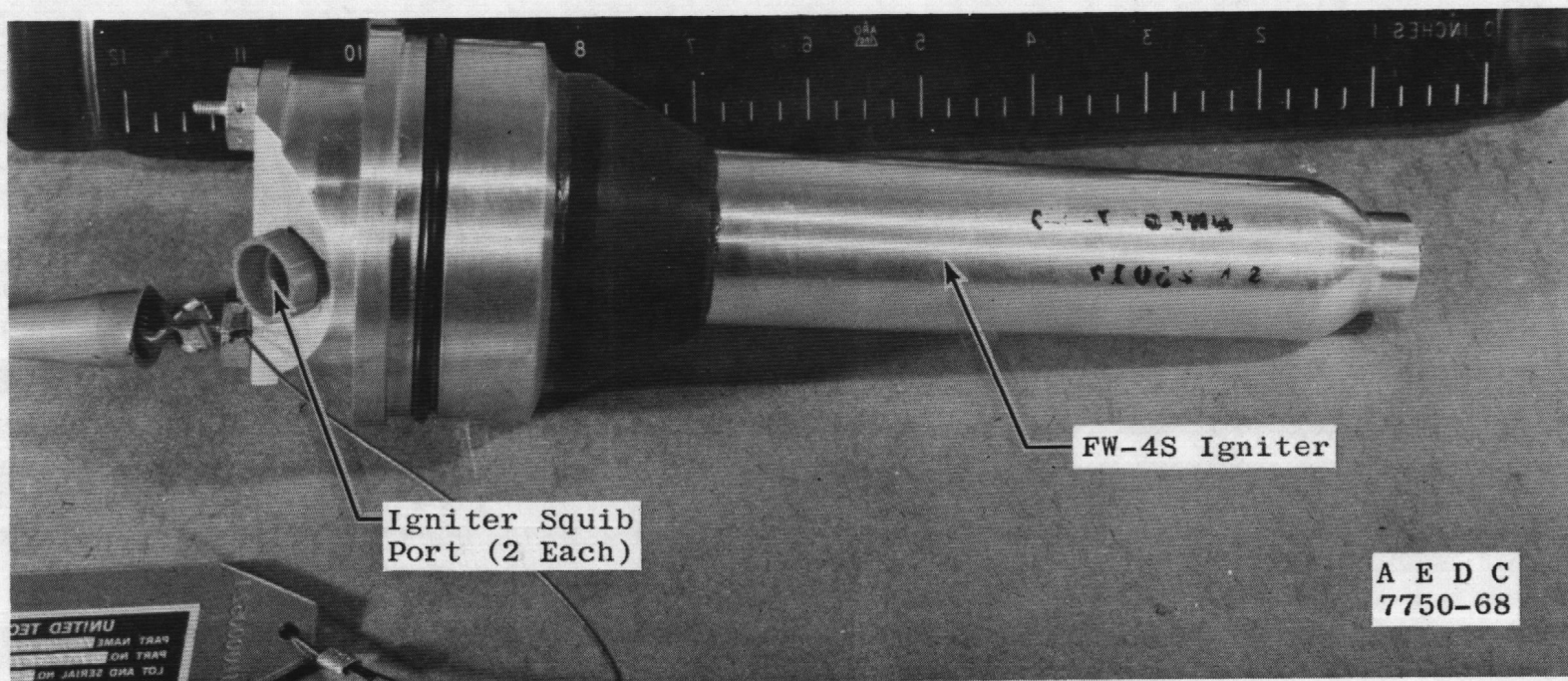2. Model Specification No. SC0104C, May 20, 1969, Rocket Motor FW-4S.

Additional Insulator (Silica-Loaded Buna-N Rubber) 0.05 in. Thick

Forward Adapter (High-Strength Aluminum)

Additional Insulator (Silica-Loaded Buna-N Rubber) 0.10 in. Thick
Propellant (UTP 3096A)

Forward Insulator (Silica-Loaded Buna-N Rubber)

Fiber Glass Case

Aft Insulator (Silica-Loaded Buna-N Rubber)

58.45

40.38

Aft Adapter (High Strength Aluminum)

20 deg

Aluminum Polar Boss

Steel

Aluminum Polar Boss

High Silica Phenolic

Area Ratio = 9:1

Graphite Cloth

Transverse Slot

4.2 Diam (Nominal)

2.344 Diam

Graph-I-Tite G-90 Throat Insert

Igniter Port

3.0 Diam (Nominal)

19.67

16.54

All dimensions are in inches.

a. Schematic
Figure 1. United Technoloty Center FW-4S rocket motor.

b. Prefire photograph
Figure 1. Concluded.

Chamber Pressure Port (Typical)

UTP 1095 Propellant

Pellet
Retainer
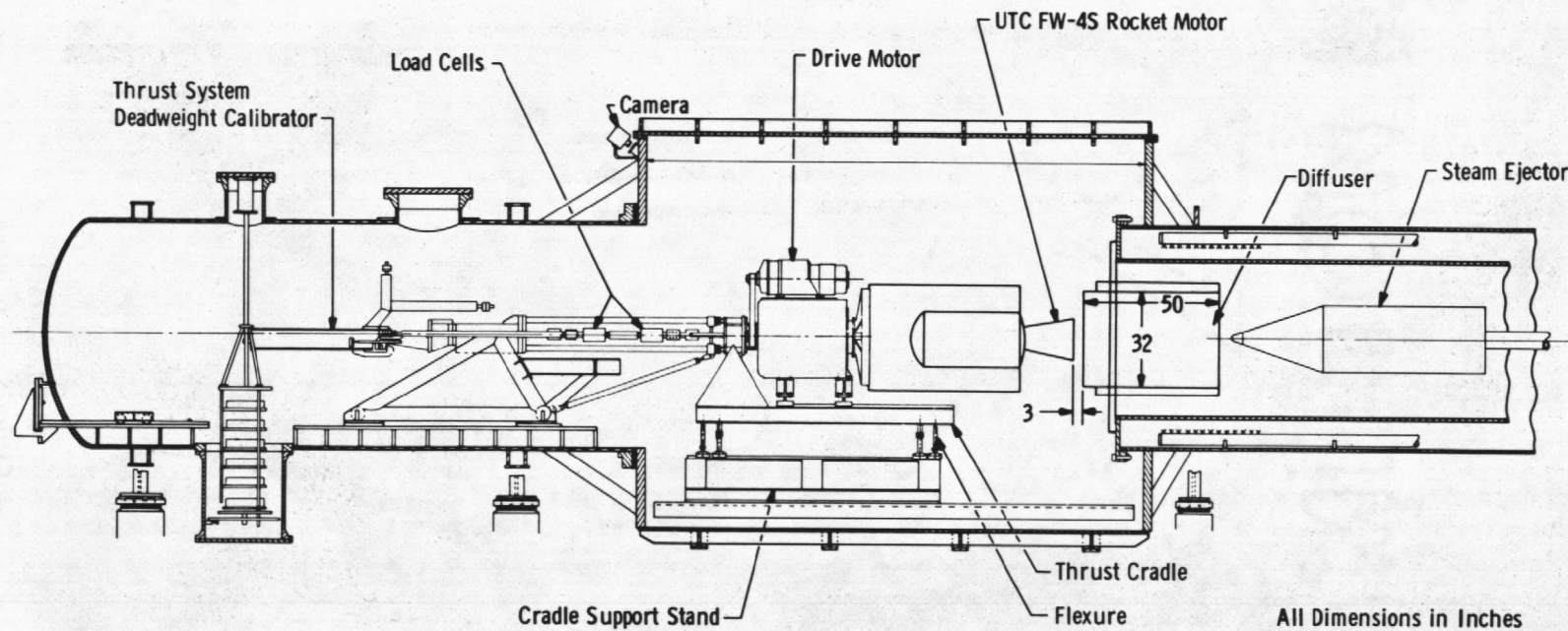Screen

BKNO$_3$
Pellets

Igniter Squib Port (Typical)

9.26 in.

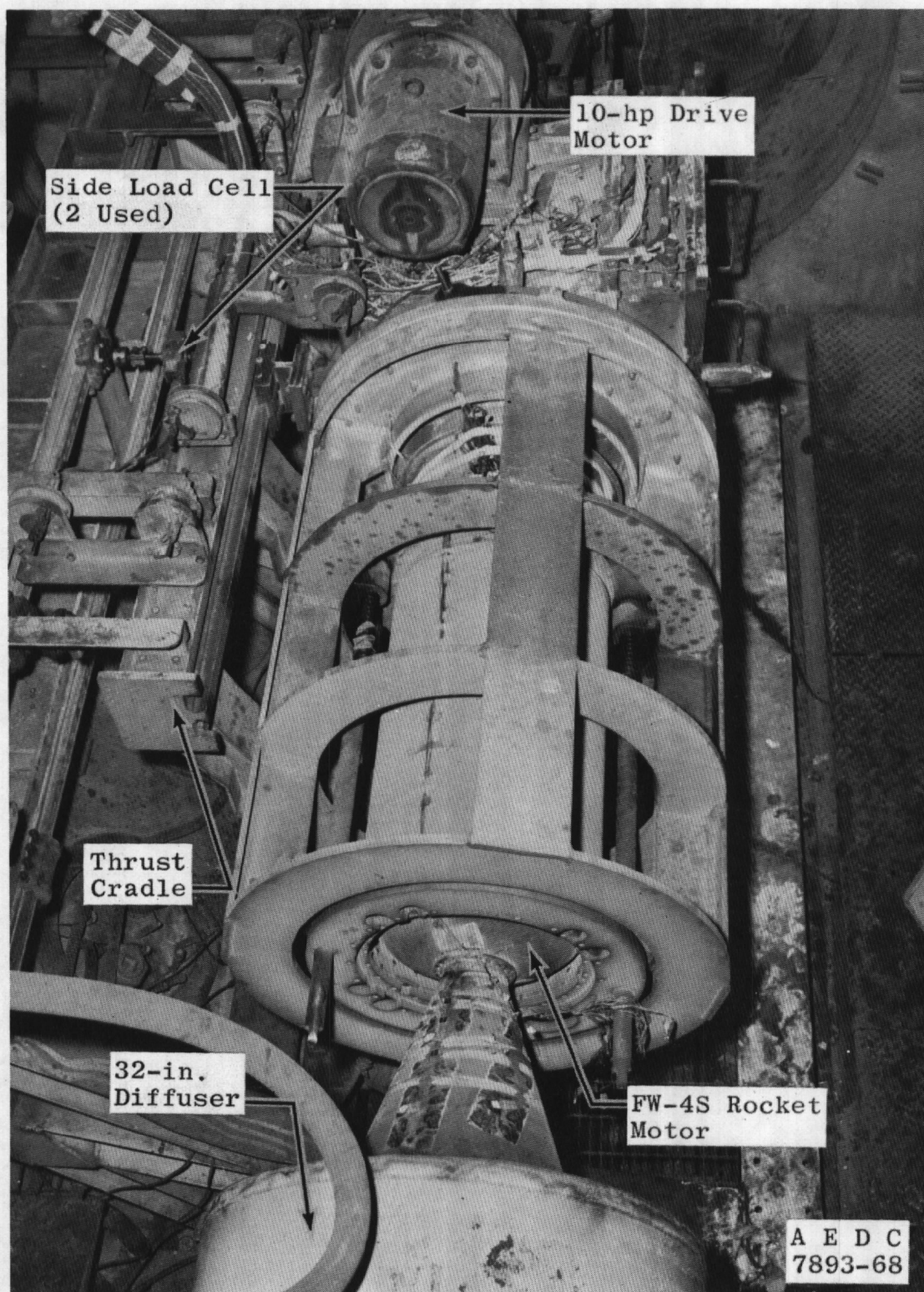a. Schematic
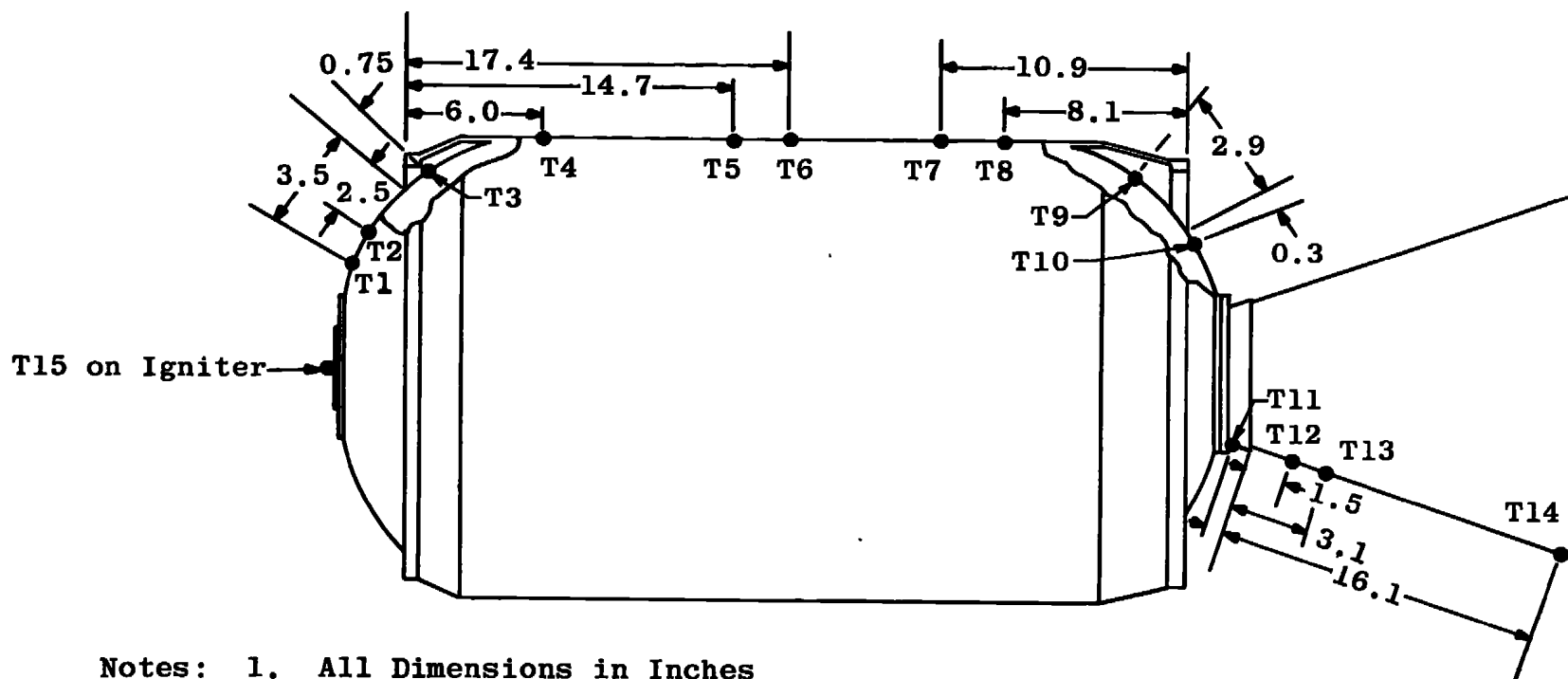Figure 2. FW-4S igniter.

b. Photograph
Figure 2. Concluded.

a. Schematic

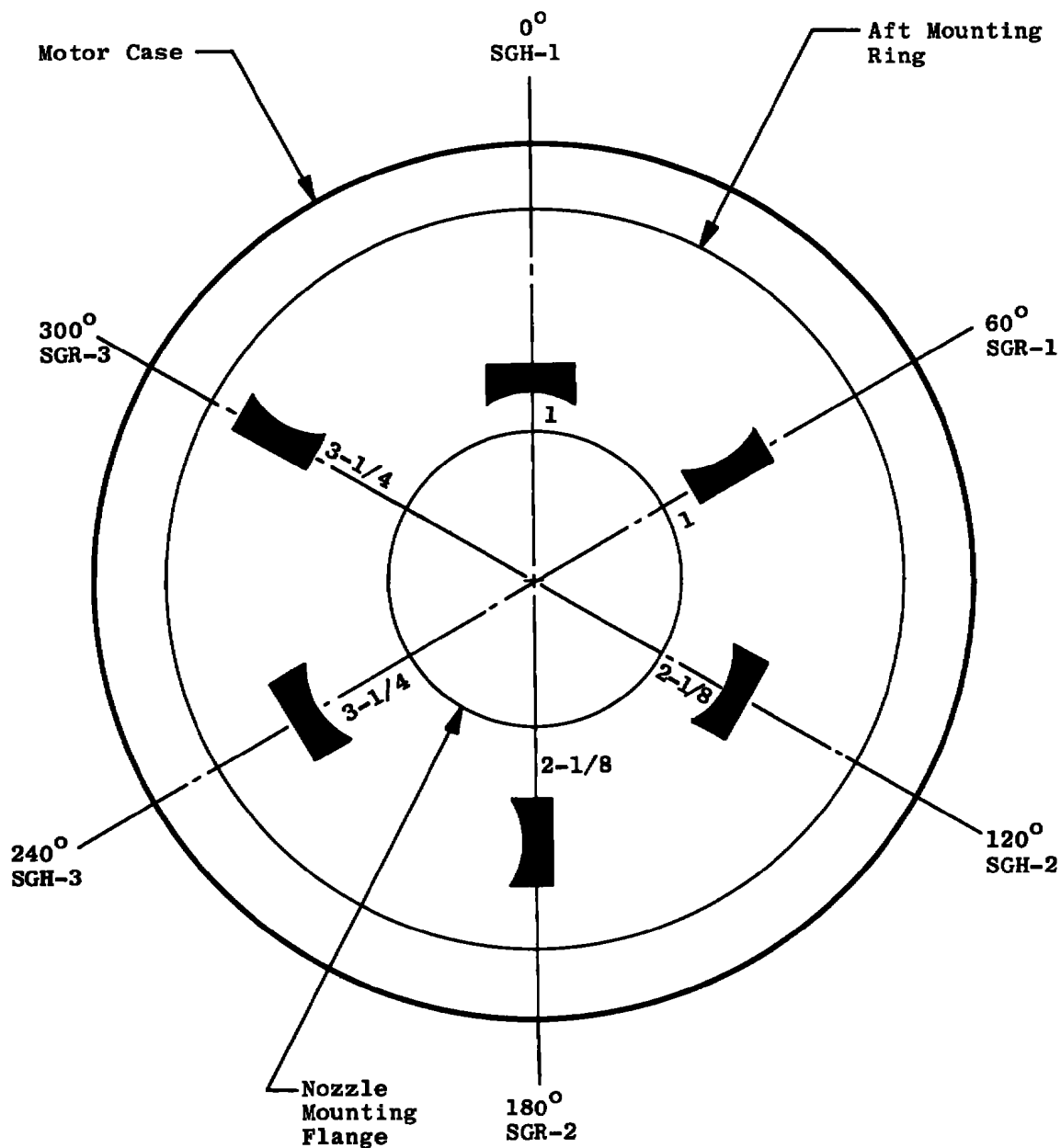Figure 3. Installation of FW-4S motor and spin assembly in Propulsion Development Test Cell (T-3).

b. Photograph
Figure 3. Concluded.

Figure 4. Thermocouple locations.

Notes: 1. All Dimensions in Inches
2. Radial Location of Thermocouples:
T1 through T11 Located at TDC
T12 through T14 Located at 180 deg
T15 N/A

UTC FW-4S Motor, Looking Upstream

Notes: 1. SGH-1, -2, -3   Measure Hoop Strain
       2. SGR-1, -2, -3   Measure Radial Strain
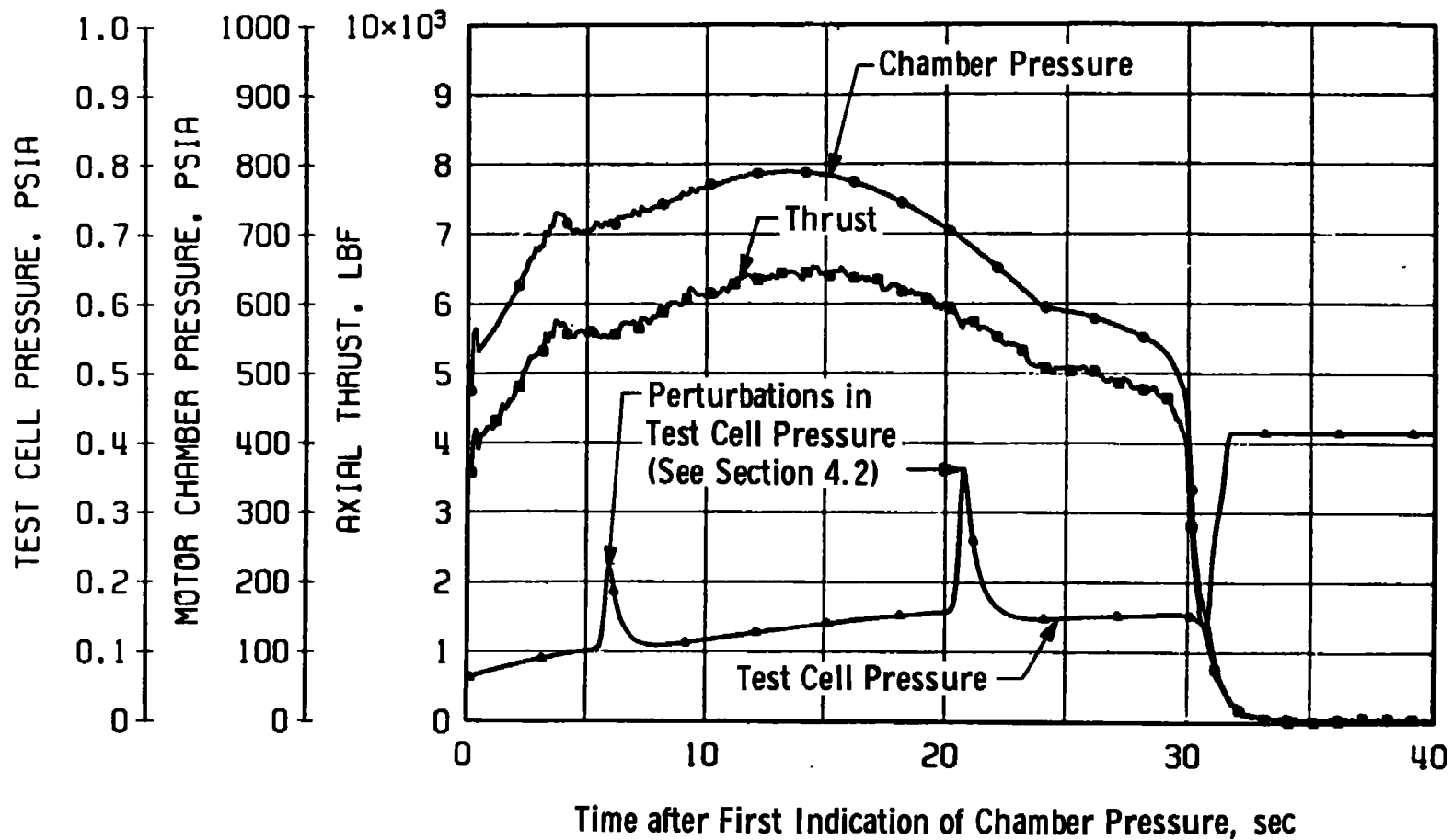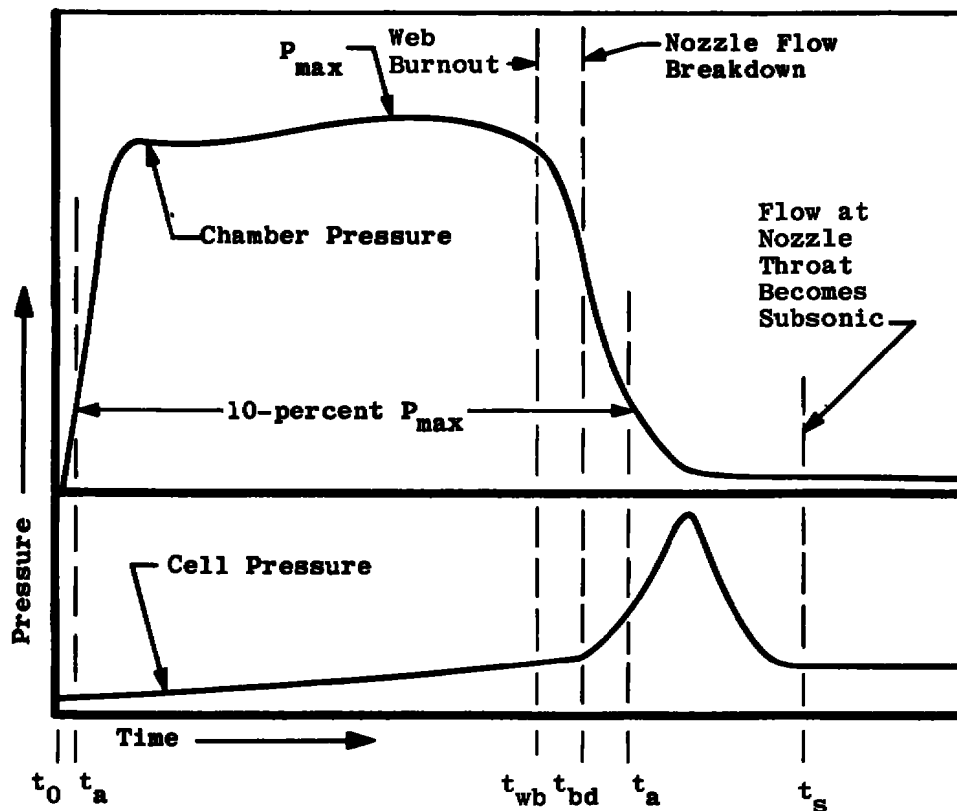   3. All Dimensions in Inches

Figure 5. Strain grid locations.

Figure 6. Variation of thrust, chamber pressure, and test cell pressure during firing.

$$I_{vac_{total}} = \int_{t_0}^{t_{bd}} F \, dt + A_{ex_{(avg)}} \int_{t_0}^{t_{bd}} P_{cell} \, dt + \bar{c}_f \, A_{th_{(post)}} \int_{t_{bd}}^{t_s} P_{ch} \, dt$$

$$I_{vac_{action}} = \int_{t_{a_{ignition}}}^{t_{bd}} F \, dt + A_{ex_{(avg)}} \int_{t_{a_{ignition}}}^{t_{bd}} P_{cell} \, dt + \bar{c}_f \, A_{th_{(post)}} \int_{t_{bd}}^{t_{a_{tailoff}}} P_{ch} \, dt$$

where: $\bar{c}_f = \dfrac{\displaystyle\int_{t_1}^{t_2} F \, dt + A_{ex_{(post)}} \int_{t_1}^{t_2} P_{cell} \, dt}{A_{th_{(post)}} \displaystyle\int_{t_1}^{t_2} P_{ch} \, dt}$, established from data

during the time interval from 28.6 to 29.6 sec after first indication of chamber pressure.

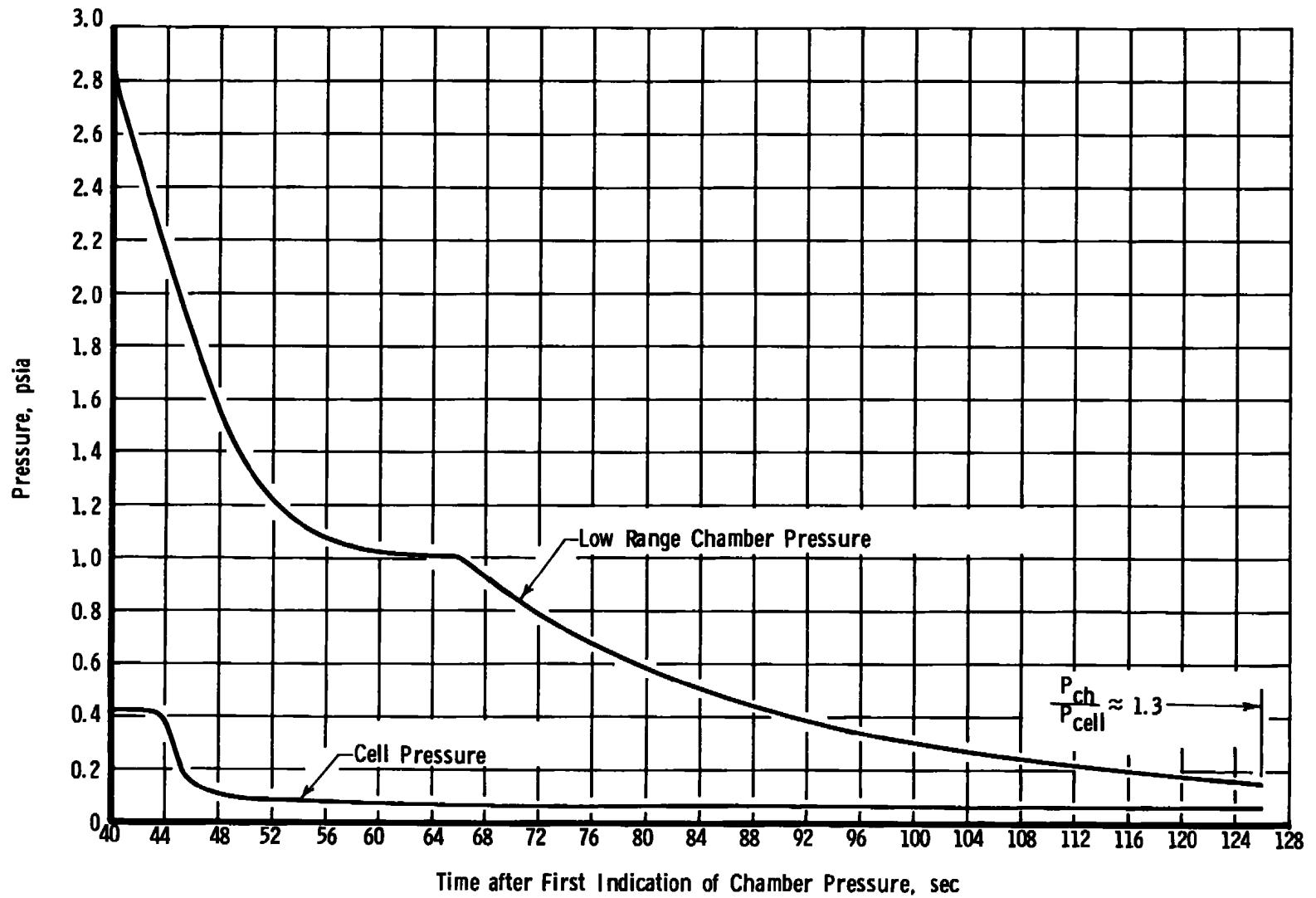Figure 7. Definition of vacuum total and action impulse.

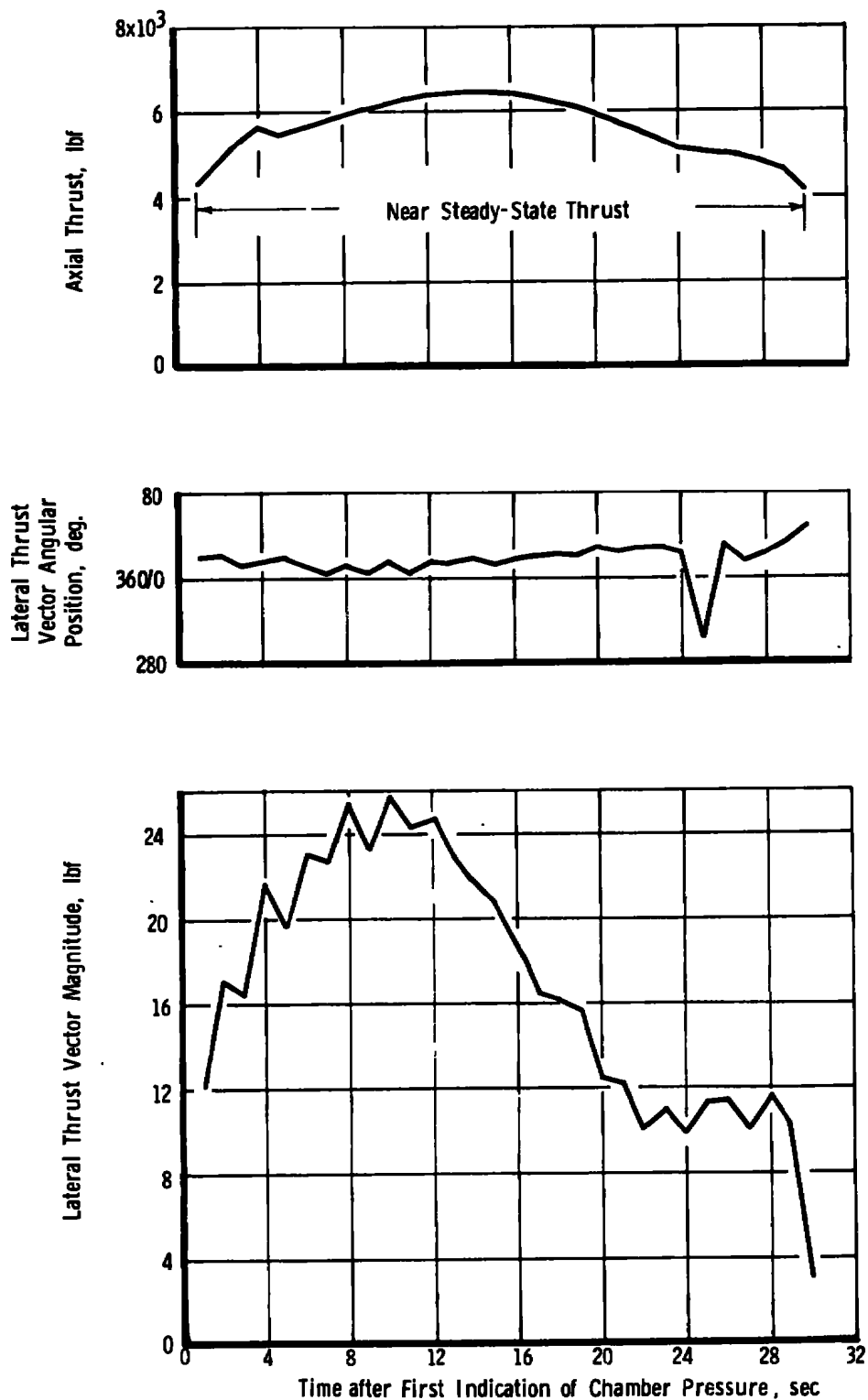Figure 8. Comparison of low-range chamber pressure and test cell pressure during motor tailoff.
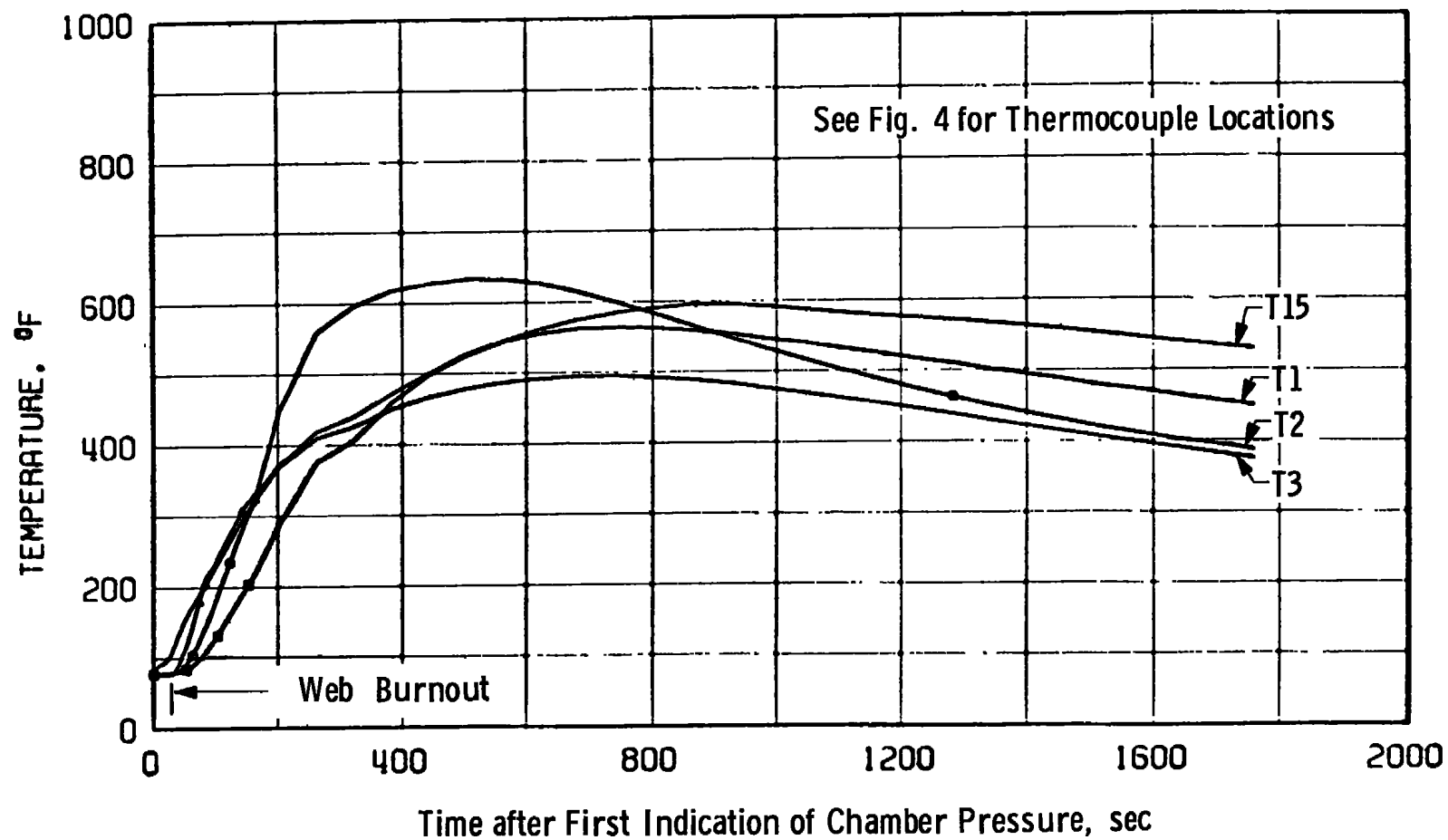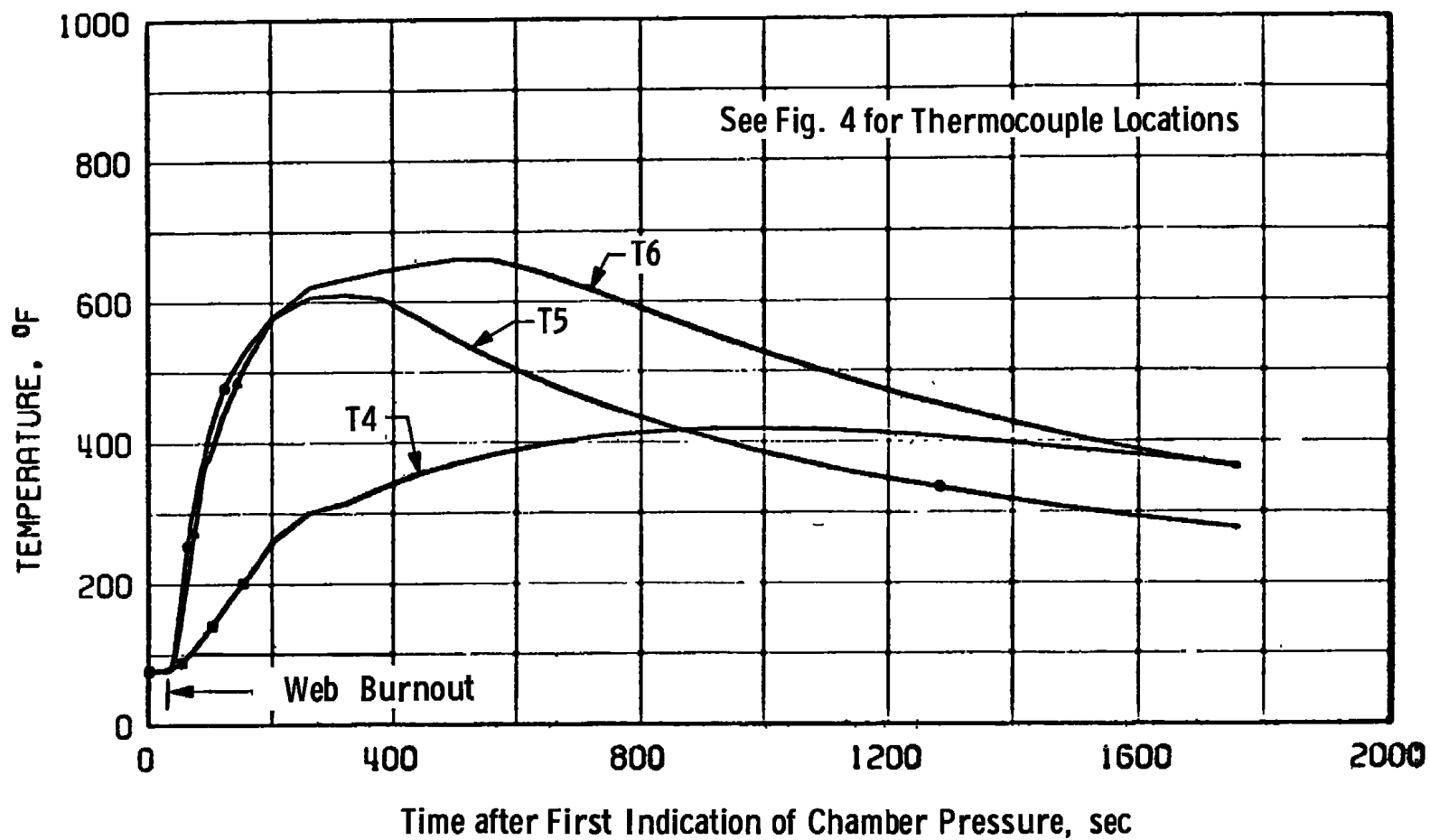
Figure 9. Variation of lateral (nonaxial) thrust vector during firing.

a. Forward dome, igniter
Figure 10. Motor temperature variation with time.

b. Motor case
Figure 10. Continued.

See Fig. 4 for Thermocouple Locations

T7

T8

Web Burnout

Time after First Indication of Chamber Pressure, sec
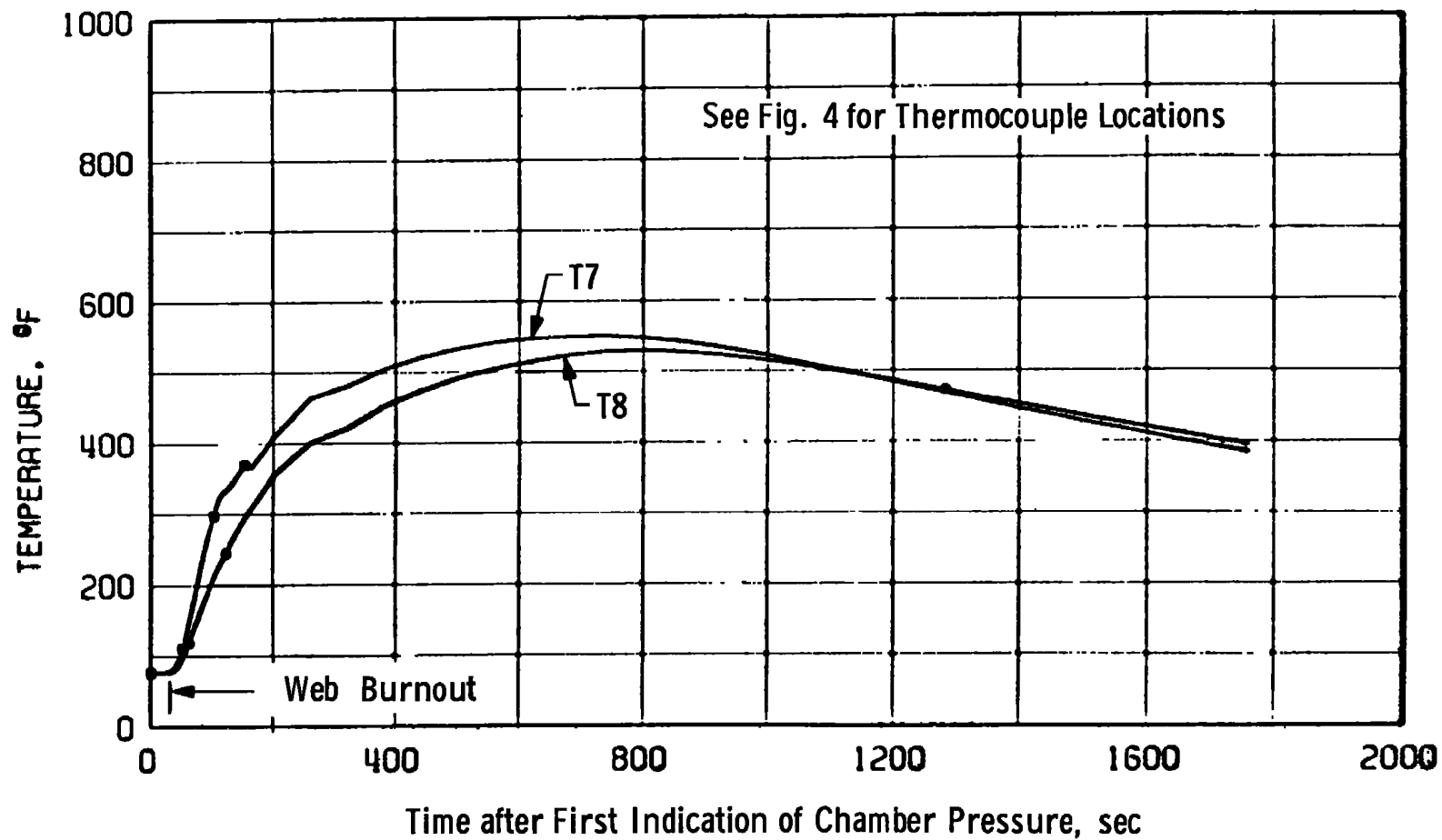
c. Motor case
Figure 10. Continued.
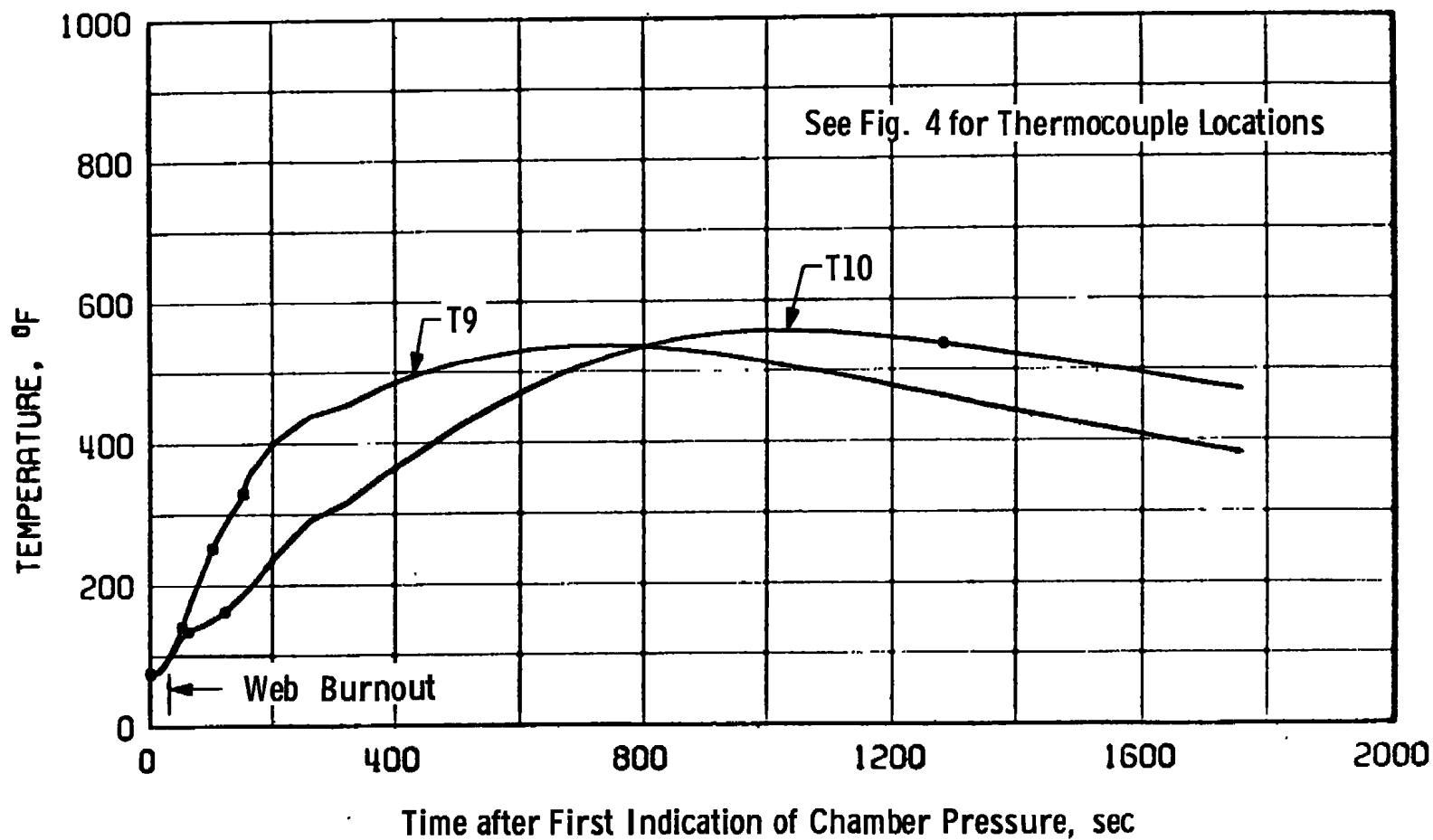
d. Aft dome
Figure 10. Continued.
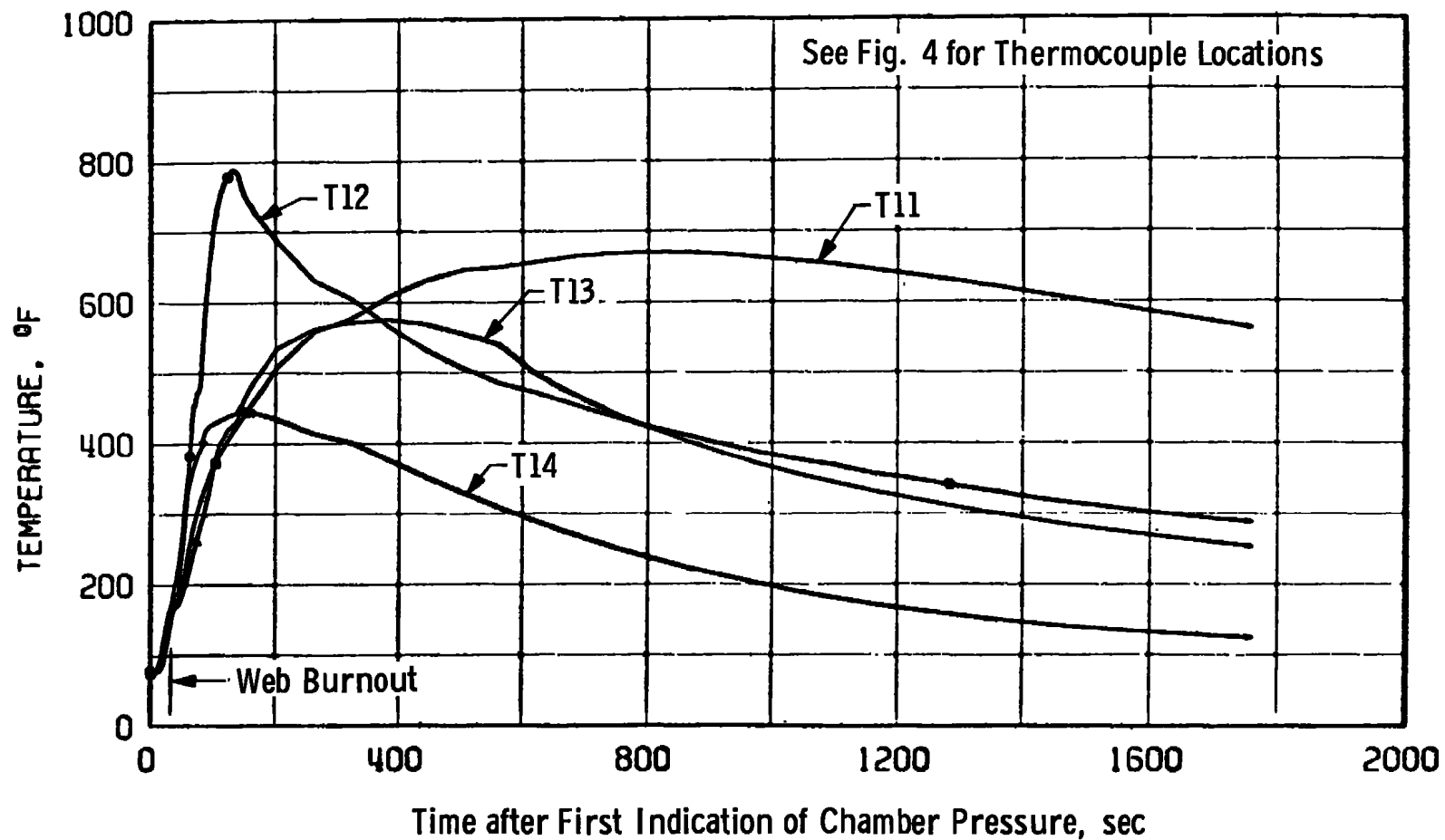
e. Nozzle
Figure 10. Concluded.
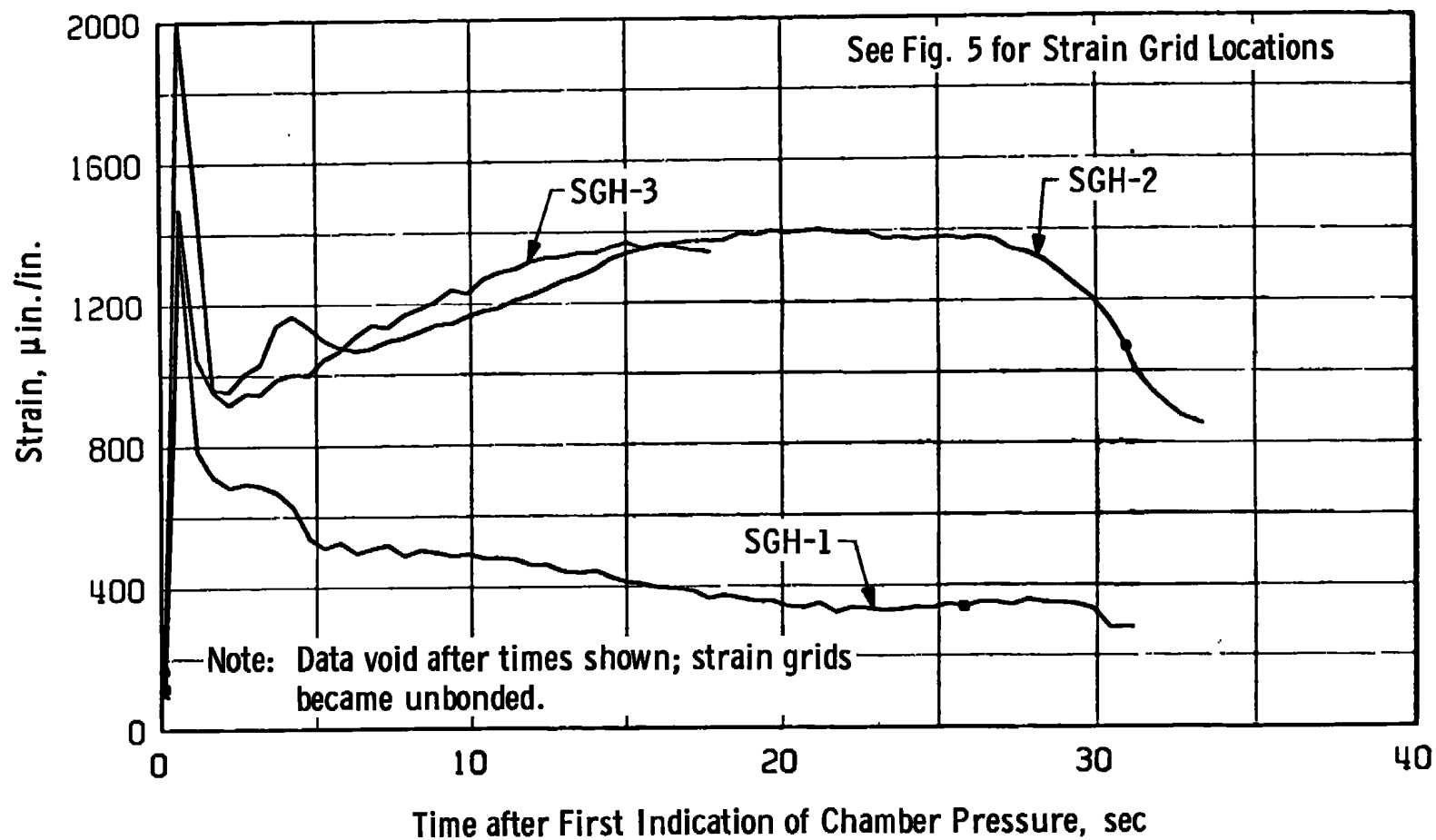
a. Hoop strain
Figure 11. Variation of aft dome strain with time.

b. Radial strain
Figure 11. Concluded.

a. Overall
Figure 12. Postfire photographs.

Delaminations

Discoloration

12 INCHES

Nozzle

b. Motor case (details)
Figure 12. Continued.

(Looking Upstream)

AEDC
3289-74

c. Nozzle exit cone interior
Figure 12. Concluded.

Table 1. Instrumentation Summary and Measurement Uncertainty

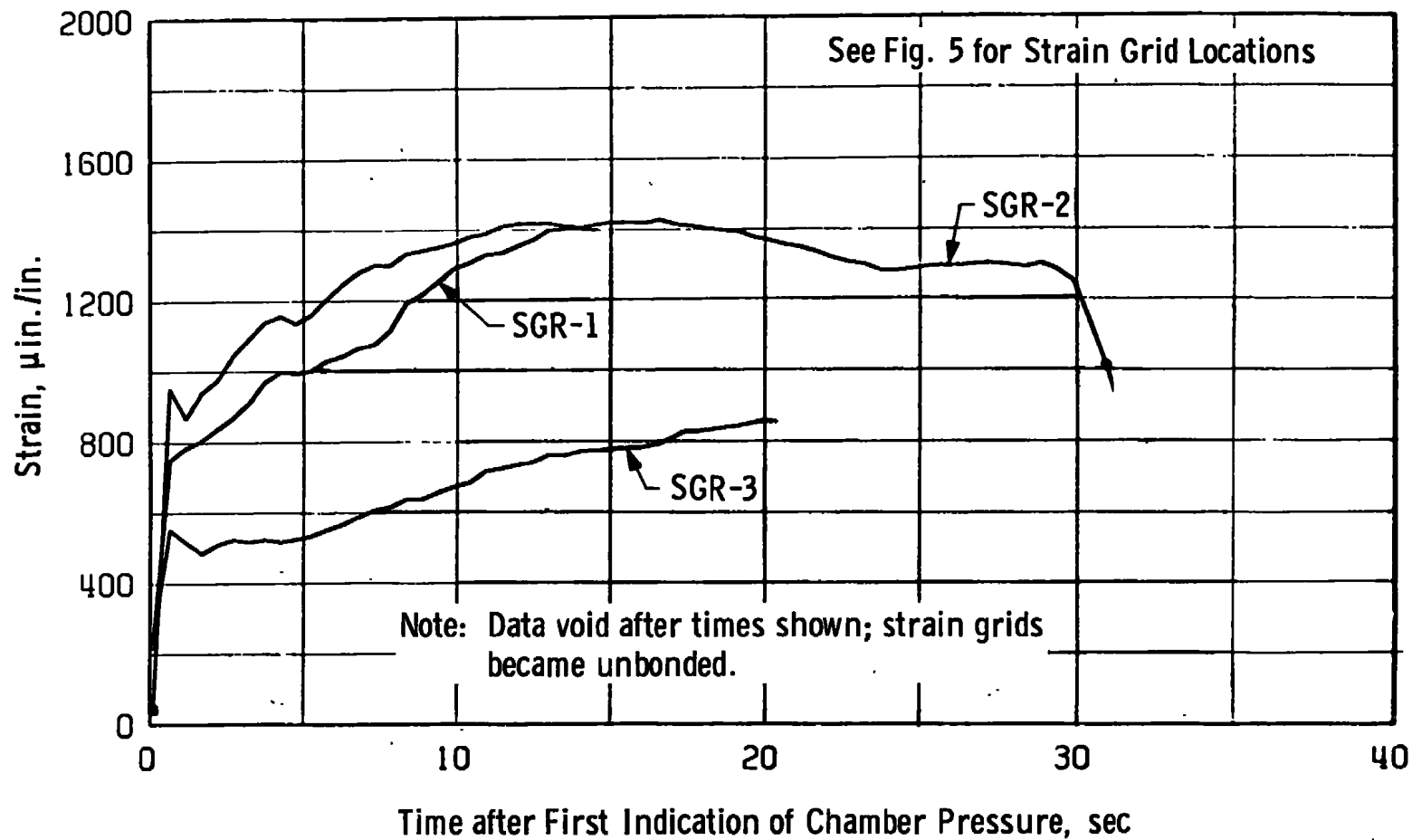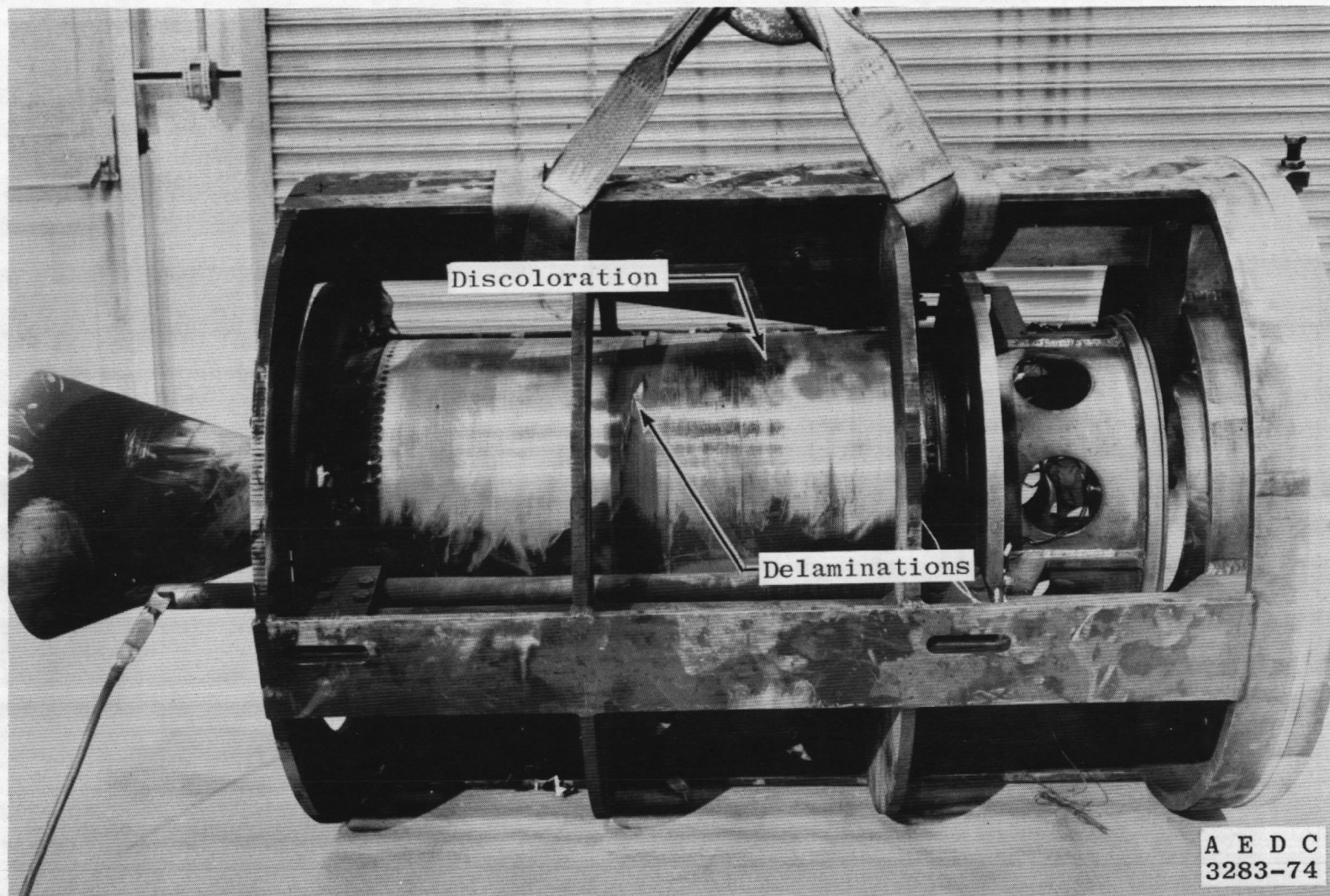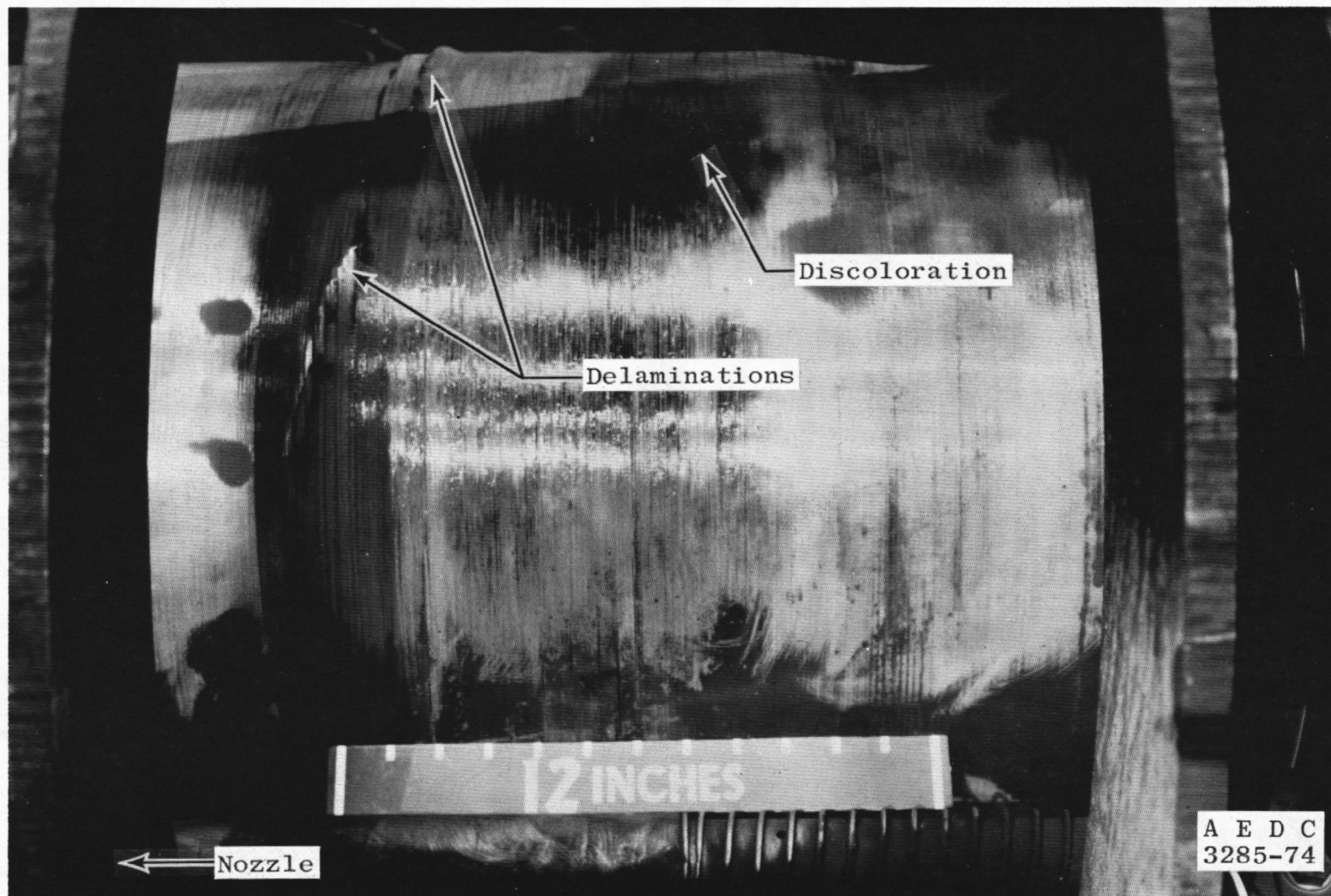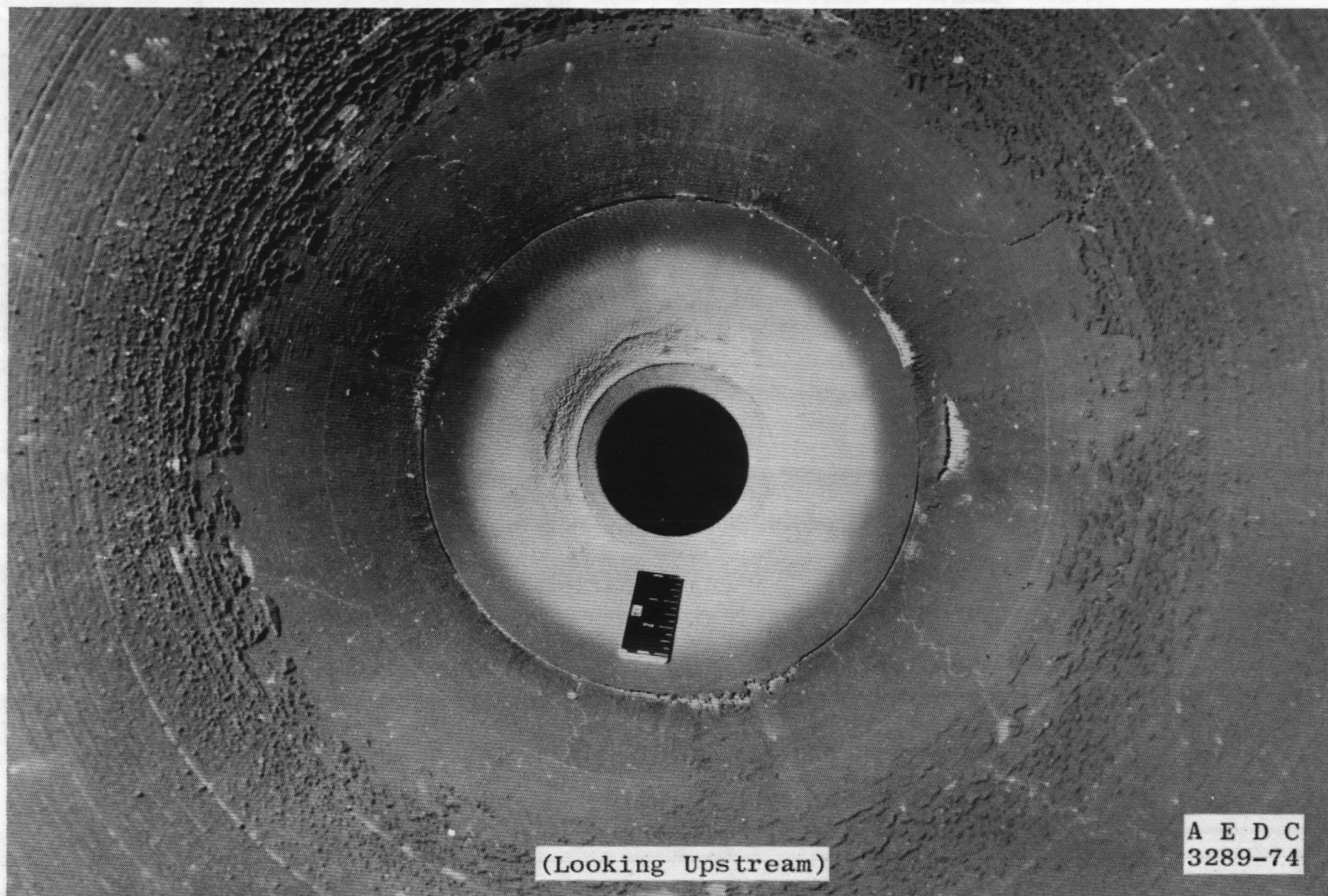| Parameter Designation	STEADY-STATE ESTIMATED MEASUREMENT*							Range	Type of Measuring Device	Type of Recording Device	Method of System Calibration
	Precision Index (S)			Bias (B)		Uncertainty ±(B + t₉₅S)					
	Percent of Reading	Unit of Measurement	Degree of Freedom	Percent of Reading	Unit of Measurement	Percent of Reading	Unit of Measurement				
Axial Force, lbf	±0.09	----	216	±0.05	----	±0.23	----	4400 to 6600 lbf	Bonded Strain-Gage-Type Force Transducers	Sequential Sampling, Millivolt-to-Digital Converter, and Magnetic Tape Storage Data Acquisition System	In-Place Application of Deadweights Calibrated in the Standards Laboratory
Total Impulse, lbf-sec	±0.07	----	31	±0.05	----	±0.19	----	----			
Chamber Pressure, psia	±0.10	----	31	±0.21	----	±0.41	----	560 to 790 psia	Bonded Strain-Gage-Type Pressure Transducers		Resistance Shunt Based on the Standards Laboratory Determination of Transducer Applied Pressure versus Resistance Shunt Equivalent Pressure Relationship
Chamber Pressure Integral, psia-sec	±0.10	----	31	±0.21	----	±0.41	----	----			
Chamber Pressure psia (low range)	----	±0.003 psia	31	----	±0.003 psia	----	±0.01 psia	0.09 to 1.5psia			
	±0.23	----	31	±0.21	----	±0.67	----	1.5 to 15 psia			
Test Cell Pressure, psia	±0.38	----	72	±1.7	----	±2.5	----	0.06 to 0.40 psia	Unbonded Strain-Gage-Type Pressure Transducers		
Test Cell Pressure Integral, psia-sec	±0.38	----	31	±1.7	----	±2.5	----	----			
Temperature, °F	----	±0.25°F	31	----	±2.2°F	----	±2.7°F	75 to 530°F	Chromel-Alumel Temperature Transducers		Millivolt Substitution Based on the NBS Temperature versus Millivolt Tables
	----	±0.25°F	31	±(0.25% + 0.9°F)		±(0.25% + 1.4°F)		530 to 800°F			
Weight, lbm	----	±0.015 lbm	31	----	±0.056 lbm	----	±0.09 lbm	800 to 1410 lbm	Beam-Balance Scales	Visual Readout	In-Place Application of Deadweights Calibrated in the Standards Laboratory
Strain Grids	±0.5	----	31	±9.	----	±10. See Note	----	150 to 1500 µin./in.	Strain Grid	Sequential Sampling, Millivolt-to-Digital Converter, and Magnetic Tape Storage Data Acquisition System	Resistance Shunt Based on the Manufacturer's Determination of Elongation versus Resistance Change

*REFERENCE: CPIA No. 180. "ICRPG Handbook for Estimating the Uncertainty in Measurements made with Liquid-Propellant Rocket Engine Systems." (AD855130), April 30, 1969.

Note: Uncertainty Estimate Based on Experience with Systems Similar to those Furnished by User.

Table 2. Summary of FW-4S Motor Performance

	Actual Performance	Specification Limits[6]
Test Number - RA307	01	---
Motor Serial Number	2501-2	---
Test Date	4/11/74	---
Motor Spin Rate, rpm	180	---
Simulated Altitude at Ignition, ft	121,000	---
Motor Case Temperature at Ignition, °F	77	---
Ignition Delay time (t_d)[1], sec	0.12	0.071 to 0.165
Action Time (t_a)[2], sec	31.12	28.4 to 32.0
Total Burn Time (t_g)[3], sec	126	---
Nozzle Flow Breakdown Time, (t_{bd})[4], sec	30.87	---
Web Burnout Time (t_{wb})[5], sec	29.30	---
Measured Total Impulse (based on t_{bd})		
Average of 4 Channels, lbf-sec	169,778	---
Maximum Channel Deviation from Average, percent	0.03	---
Cell Pressure Integral (based on t_{bd})		
Average of 2 Channels, psia-sec	4.237	---
Maximum Channel Deviation from Average, percent	0.47	---
Chamber Pressure Integral (based on t_{bd})		
One Channel Only, psia-sec	20,692	---
Chamber Pressure Integral		
(Based on t_a), psia-sec	20,724	---
(Based on t_g), psia-sec	20,836	---
Vacuum Thrust Coefficient (based on 1-sec of data prior to tailoff), $\overline{C}_f$	1.844	---
Vacuum Total Impulse		
(Based on t_a), lbf-sec	170,935	171,600 to 174,020
(Based on t_g), lbf-sec	172,024	---
Average Simulated Altitude (based on t_a), ft	103,000	---
Vacuum Specific Impulse, lbf-sec/lbm		
(Based on t_g and Manufacturer's Stated Propellant Weight)	284.34	---
(Based on t_g and AEDC Expended Mass)	284.59	---
Average Vacuum Thrust Coefficient, C_F (Based on t_a and Average of Pre- and Postfire Throat Area)	1.831	---

[1]Ignition Delay Time, time interval from first indication of chamber pressure until chamber pressure has risen to 90 percent of maximum.

[2]Action Time, time interval between 10 percent of maximum chamber pressure during ignition and 10 percent of maximum chamber pressure during tailoff.

[3]Total Burn Time, time interval between first indication of chamber pressure during ignition and the time at which the ratio of chamber pressure to cell pressure had decreased to 1.3 during tailoff.

[4]Nozzle Flow Breakdown Time, the time after ignition when exhaust diffuser flow breakdown occurs, as indicated by an abrupt increase in cell pressure during tailoff.

[5]Web Burnout Time, the time abscissa of the intersection of the pressure-time curve with the bisector of the angle between the tangents of the final level portion and of the descending portion of the curve.

[6]Specification limits are for a motor conditioned at 70°F and spinning at 200 rpm.

Table 3. Summary of FW-4S Motor Physical Dimensions

Test Number	RA307-03
Motor Serial Number	2501-2
Test Date	4/11/74
AEDC Prefire Motor Weight, lbm[1]	1409.08
AEDC Postfire Motor Weight, lbm[1]	804.62
AEDC Expended Mass, lbm	604.46
Manufacturer's Stated Propellant Weight, lbm	605.00
Nozzle Throat Area, in.^{2}	
Prefire	4.277
Postfire[2]	4.742
Percent Change from Prefire Measurement	10.87
Nozzle Exit Area, in.^{2}	
Prefire	215.51
Postfire	215.89
Percent Change from Prefire Measurement	0.18

[1]Includes igniter and firing harness.
[2]Exhaust products not removed prior to measurements.

Table 4. Comparison of Performance with Previous FW-4S Motor Firing

	Current Test	Previous Test (Ref. 1)
Motor S/N	2501-2	2218-9
Conditioning Temperature, °F	75 ± 5	75 ± 5
Spin Rate, rpm	180	180
Action Time, sec	31.1	33.0
Vacuum Total Impulse		
Based on t_a	170,935	172,958
Based on t_s	172,024	173,397
Vacuum Specific Impulse, lbf-sec/lbm		
Based on Manufacturer's Stated Propellant Weight and t_s	284.34	285.74
Vacuum Specific Impulse, lbf-sec/lbm		
Based on AEDC Expended Mass and t_s	284.59	283.88
Manufacturer's Stated Propellant Weight, lbm	605.00	606.83
AEDC Expended Mass, lbm	604.46	610.81

NOMENCLATURE

C_F — Average vacuum thrust coefficient

$\bar{c}_f$ — Vacuum thrust coefficient

$I_{vac_{action}}$ — Vacuum impulse based on action time

$I_{vac_{total}}$ — Vacuum impulse based on total burn time

t_a — Action time, the time interval between 10 percent of maximum chamber pressure during ignition and 10 percent of maximum chamber pressure during tailoff

t_{bd} — Nozzle flow breakdown time, the time after ignition when exhaust diffuser flow breakdown occurs, as indicated by an abrupt increase in cell pressure during tailoff

t_d — Ignition delay time, the time interval from first indication of chamber pressure until chamber pressure has risen to 90 percent of maximum

t_o — Time of first indication of chamber pressure

t_s — Total burn time, the time interval between the first indication of chamber pressure during ignition and the time at which the ratio of chamber-to-cell pressure decreased to 1.3 during tailoff

t_{wb} — Web burnout time, the time abscissa at the intersection of the chamber pressure-time curve with the bisector of the angle between the tangents of the final level portion of the chamber pressure-time curve and of the descending portion of the curve